Motion Artifact Cancellation for Wearable Photoplethysmographic Sensor

by

Yuta Kuboyama

B.S., Electrical Engineering and Computer Science, MIT, 2009

Submitted to the Department of Electrical Engineering and Computer Science
in partial fulfillment of the requirements for the degree of

Master of Engineering in Electrical Engineering and Computer Science

at the

Massachusetts Institute of Technology

September 2010

Author .....
Department of Electrical Engineering and Computer Science
July 9, 2010

Certified by .....
Rosalind W. Picard
Professor of Media Arts and Sciences
Thesis Supervisor

Certified by .....
Richard Fletcher
Research Scientist, MIT Media Laboratory
Thesis Supervisor

Accepted by .....
Christopher J. Terman
Chairman, Department Committee on Graduate Theses

Motion Artifact Cancellation for Wearable Photoplethysmographic Sensor

by

Yuta Kuboyama

Submitted to the Department of Electrical Engineering and Computer Science
July 9, 2010
in partial fulfillment of the requirements for the degree of
Master of Engineering in Electrical Engineering and Computer Science

Abstract

Photoplethysmography (PPG) is a non-invasive and unobtrusive technique to measure heart rate from the surface of the skin, by exposing a section of the skin to an LED light and measuring the changes in reflected light due to the blood pulsing through under the skin. However, PPG signals are highly susceptible to motion artifacts, and in order for this technique to be useful for heart rate measurements around-the-clock, a motion artifact cancellation mechanism must be implemented to recover the blood volume pulse (BVP) from the corrupted signal. Various digital signal processing (DSP) approaches for motion artifact cancellation have been attempted in the past, but a reliable around-the-clock PPG sensor is yet to be out on the market. This thesis outlines a novel, analog implementation of the motion artifact cancellation system, to evaluate the impact of sensor front-end improvements on the performance of motion artifact cancellation.

Thesis Supervisor: Rosalind W. Picard
Title: Professor of Media Arts and Sciences

Thesis Supervisor: Richard Fletcher
Title: Research Scientist, MIT Media Laboratory

Acknowledgments

First of all, I would like to thank my thesis advisors Professor Rosalind Picard and Dr. Rich Fletcher for their support and mentorship throughout my M.Eng program. This project would not have been successful without their guidance, and I am extremely grateful for this great research opportunity that they have offered me as my M.Eng thesis project.

I would also like to thank Professor Joseph Paradiso and Dr. Mark Feldmeier from the Responsive Environments Group at the MIT Media Lab, for their advice and technical expertise on the design of the automatic gain control system used in the motion artifact cancellation design.

I would like to thank all of the members of the Affective Computing Group, and in particular, I would like to thank Ming-Zher Poh for his advice and insights on physiological sensing, and for spending numerous hours in heated discussions for various sensor design considerations.

I would like to express my sincere gratitude to Nancy Lurie Marks Family Foundation and National Institutes of Health (project number 1RC1DA028428-01) for making this project possible by generously providing financial support.

Finally, I would like to thank my family and friends, without whom none of this would have been possible.

Contents

List of Figures

Chapter 1

Introduction

1.1 Motivation

Physiological sensing using wearable biosensors is a research field that has gained attention due to its potential for revolutionizing healthcare, by enabling pervasive physiological monitoring using relatively low-cost devices. In particular, there is currently great interest in being able to monitor heart rate around-the-clock for various medical applications. For example, for those who are on the autism spectrum who have difficulties communicating emotional state, rapid increases in heart rate during a nervous meltdown may be monitored to inform others in the vicinity to assist in calming the person down [1]. Similarly, for those diagnosed with epilepsy, a record of heart rate during a seizure may provide insight into such conditions, and the knowledge gained from this may potentially lead to the development of technologies for seizure detection and prediction [2].

It is important for such biosensors to enable continuous, non-invasive, and unobtrusive means for monitoring heart rate comfortably during regular, day-to-day activities. However, currently the most common method for continuously monitoring heart rate is by the use of electrocardiogram (ECG), which involves attaching a pair of electrodes across the user's chest to measure the electrical activity of the heart. This is clearly an obtrusive approach, especially when the sensor must be worn continuously for many days in a row.

Photoplethysmography (PPG) is an alternative measurement approach that detects the blood volume pulse (BVP) using an electro-optical technique [3]. A section of the skin is illuminated using a light source, and a change in the reflected light is detected as the blood pulses through underneath the skin. This technique is often used for heart rate measure-

ments off the fingertips or the wrist. It is a comfortable, non-invasive, and unobtrusive approach that has existed for many years, and is an appealing technique for around-the-clock heart rate measurements.

1.2 The Photoplethysmography Model

Photoplethysmography is one of the least obtrusive methods that can detect BVP off a person's skin. With the PPG technique, a light source (usually an infra-red LED) is used to illuminate a section of the skin, and a photodetector (usually a photodiode or a phototransistor) is used to detect the slight volumetric change under the skin as blood pulses through underneath it and causes a change in the reflected light from the skin. This signal detected by the photodetector is then passed through a high-gain stage and amplified to produce a BVP signal as shown in the figure.

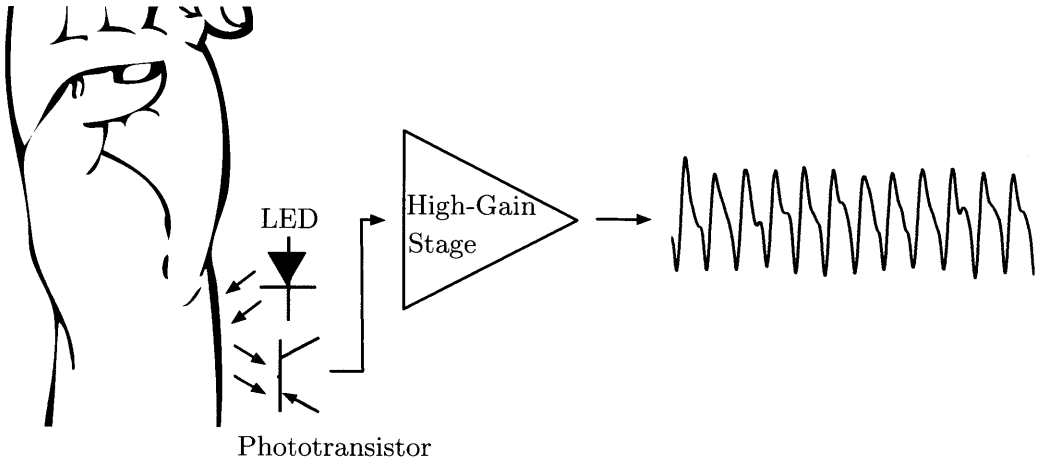

Figure 1-1: Photoplethysmography.

However, the inherent weakness behind PPG is that in addition to the volumetric changes caused by the blood pulse, there are many other factors that contribute to the overall signal. The complete PPG signal can be modelled by the expression [4]

$$S_{PPG} = S_{ambient} + S_{vascular} + S_{mechanical} + S_{electrical} \tag{1.1}$$

$S_{ambient}$ is the influence of changes in ambient light that is detected by the photodetector. $S_{vascular}$ is known as vascular dynamics, which is caused by volumetric changes and pressure wave propagation under the skin. This includes our signal of interest, which is the volumetric

change caused by the blood pulse (BVP), but it also includes propagating pressure waves due to respiration and other muscle movements that occur anywhere in the body. $S_{mechanical}$ is the effect of sensor movement (ie slight changes in placement and orientation of the LED and the photodetector that occur as a result of user movement) relative to the skin. Finally, $S_{electrical}$ is the effect of electrical noise that exists in the sensor hardware, such as ripple in the power supply rail.

Therefore the PPG signal is a complex mixture of various components, and it is impossible to extract the signal of interest (BVP) by simple frequency isolation, or by attempting to fully characterize the entire signal. This is essentially a signal isolation problem, where the signal of interest must be isolated from a "black box" mixture of various components. $S_{ambient}$ can be minimized by isolating the LED and the photodetector from all external light sources, and $S_{electrical}$ can be minimized by applying proper circuit design techniques. Therefore, the PPG signal can be reduced to $S_{vascular}$ and $S_{mechanical}$, which are both consequences of some form of movement, either internal (blood pulse, respiration, muscle movements, etc) or external (sensor placement shift due to motion). Since the BVP is our signal of interest, we can combine all other components as "motion artifacts", and rewrite the PPG expression as

$$S_{PPG} = S_{BVP} + S_{motion\_artifact} \tag{1.2}$$

Therefore in order to develop a practical heart rate sensor using PPG, a motion artifact cancellation system must be implemented to recover the BVP signal. Throughout the rest of this thesis, BVP and motion artifacts will be addressed as "signal" and "noise" respectively, for the ease of explanation.

1.3 Motion Artifact Cancellation

As mentioned previously, motion artifact cancellation is essentially a signal isolation problem, where the signal of interest is buried inside a "black box" mixture of motion artifacts. One may at first assume that the motion artifacts can be modelled by tracking the sensor motion using an accelerometer. However, this is clearly insufficient, as motion artifacts induced by propagating pressure waves from respiration and muscle movements may not be detected by the accelerometer. Various digital signal processing (DSP) techniques have been attempted in the past, such as active noise cancellation (adaptive feedback) [3, 5], and

blind source separation (principal component analysis [6], independent component analysis [7]). However, the performance of such techniques have been limited, and a reliable PPG based heart rate sensor for around-the-clock monitoring is yet to be out on the market. It is also important to note that many of the DSP motion artifact cancellation approaches were implemented in post-processing, as such DSP algorithms require the use of signal history, and are also demanding in terms of computational power.

Since the improvements with the DSP motion cancellation techniques have been limited, it may instead be beneficial to redesign the PPG technique completely from the analog front-end, to obtain a cleaner BVP signal even before the signal is sampled. If a significant portion of the signal recovery can be implemented in the analog domain, the BVP signal can be recovered in real-time, and it will also allow the digital system to work with a much cleaner input signal, which can then be improved further using DSP. Therefore, the following chapters outline a novel motion artifact cancellation approach, implemented using a fully redesigned PPG analog front-end.

Chapter 2

Theory

As mentioned in the previous chapter, the use of photoplethysmographic signal for non-invasive, unobtrusive measurement of heart rate has existed for many years, but its application for around-the-clock logging of heart rate has been limited due to its susceptibility to motion artifacts. Various forms of motion artifact cancellation techniques have been attempted in the past. However, many of such approaches require extensive use of digital signal processing (DSP), and this is often only possible in post-processing (or with some amount of delay) due to the use of signal history in many of the DSP algorithms. Also, despite the fact that many DSP algorithms have been developed for motion artifact cancellation, adequate performance has not been achieved for a reliable PPG logger to be out on the market. Instead of further improving the post-processing algorithms, there may be significant benefits to redesigning the PPG sensor front-end. Motion artifact cancellation can potentially have improved performance and be implemented for real-time operation using a concept that is very well known in the analog domain: differential measurement and common-mode rejection.

2.1 Differential Measurement and Common-Mode Rejection

From an analog designer's point of view, the first approach that comes to mind for a noise cancellation system would be to apply differential measurement and common-mode rejection. The underlying concept of this approach is very simple: if we take the difference between two signals, any noise that is common to both signals will be eliminated. To illustrate this mathmatically using basic algebra, consider two voltage signals v_1 and v_2,

with valid signal components s_1 and s_2 respectively, and with common-mode noise n

$$v_1 = s_1 + n \tag{2.1}$$

$$v_2 = s_2 + n \tag{2.2}$$

The voltage difference v_d of these 2 signals is then given by

$$v_d = v_1 - v_2 = (s_1 + n) - (s_2 + n) = s_1 - s_2 \tag{2.3}$$

As shown above, the common-mode noise n is eliminated through a differential measurement.

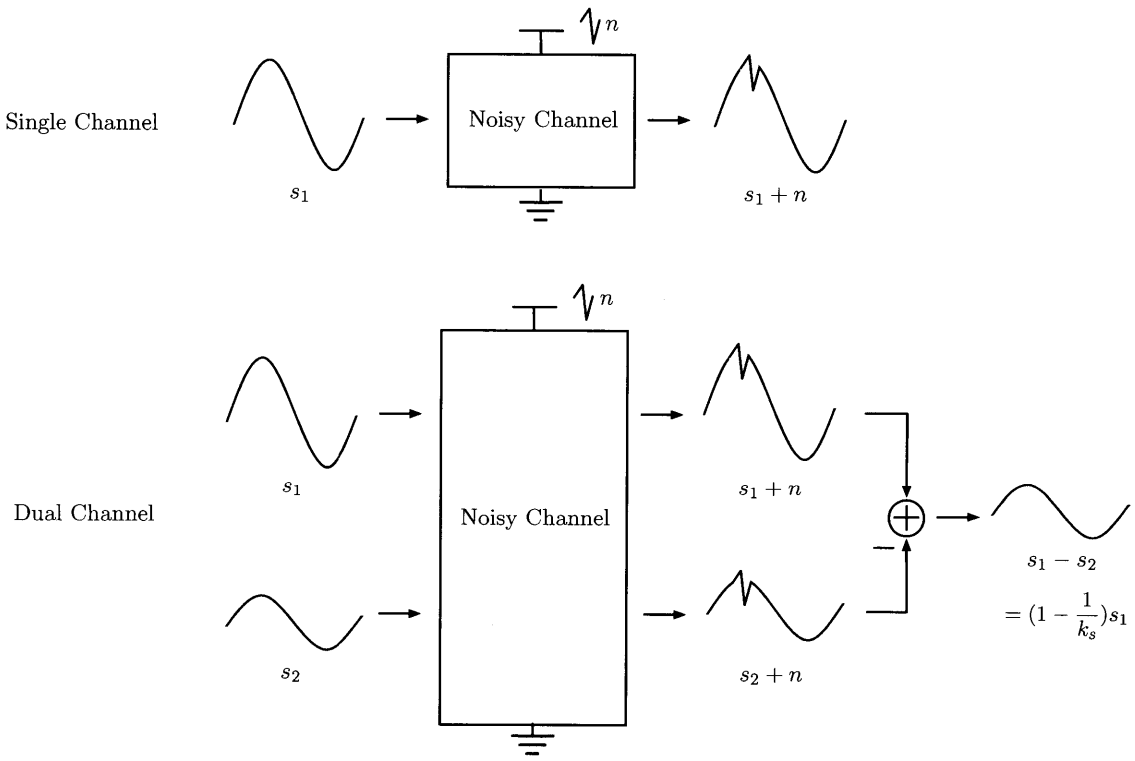

Figure 2-1: Differential measurement and common-mode rejection.

An example of this approach is shown in the figure. Imagine a signal s_1 going through a channel with a noisy power supply rail. In the single channel case, the noise n from the power supply is added onto the signal s_1 and the resulting output signal is contaminated as $s_1 + n$. However, if we add another channel with a signal s_2 that is a scaled down version of

the first signal (ie the case when $s_1 = k_s s_2$, where k_s is some scale factor greater than one), the common power supply noise n will affect both channels equivalently, and the difference v_d between the two channel outputs will produce a scaled version of the original signal s_1 with no noise content.

$$v_d = (s_1 + n) - (s_2 + n) = s_1 - \frac{s_1}{k_s} = (1 - \frac{1}{k_s})s_1 \tag{2.4}$$

This approach is very common in analog design and continuous-time signal processing, including operational amplifier design (which are differential amplifiers), and the basic building blocks of many noise cancelling headphones.

2.2 Differential Measurement Setup For PPG Signals

In order to perform a differential measurement with PPG signals, we need to develop a method to measure two signals with different BVP amplitudes, while having equivalent noise content. Differential PPG signals may be obtained by placing the LEDs and photodetectors in an asymmetric manner, as shown in the figure below[1].

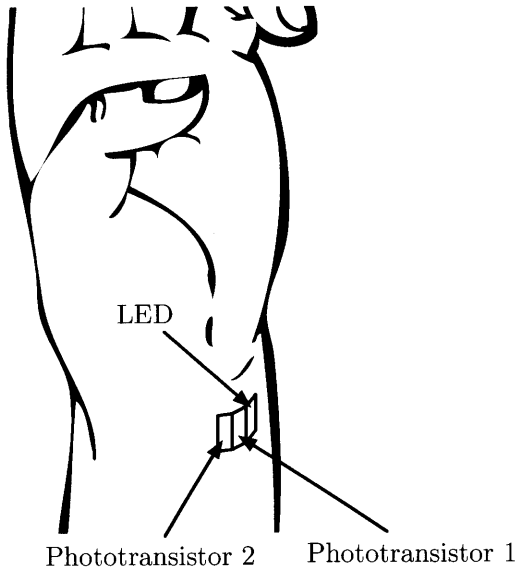

Figure 2-2: Differential measurement setup using asymmetric placement.

Two identical photodetectors are placed next to each other, and an LED is placed on

[1]Please refer to Appendix A "Alternative Differential Measurement Approaches" for alternative designs.

one end such that one of the photodetectors will be closer to the LED than the other. This will cause a difference in signal-to-noise ratio (SNR) between the two photodetectors, as brighter light source improves the SNR of the PPG signal [8]. The photodetector closer to the LED will have a better SNR compared to the photodetector that is further away from the LED. This allows us to obtain a differential signal from two identical photodetectors, which would maximize the matching of the noise content.

However, preliminary tests indicated that the matching was insufficient for the noise content to cancel out completely in a simple differential measurement. To express this mathmatically, the two PPG channels are of the form

$$v_1 = s_1 + n_1 \tag{2.5}$$

$$v_2 = s_2 + n_2 \tag{2.6}$$

and the noise components are not identical

$$n_1 \neq n_2 \tag{2.7}$$

The simple differential measurement is highly effective when the noise source is identical (eg. noisy common power rail, noisy common ground, etc). However, since the PPG signals are obtained from two separate photodetectors, there is enough manufacturing mismatch (and also placement mismatch) to ruin the differential measurement.

Although the simple differential measurement may not be sufficient in this case, as long as the noise components are scaled versions of each other (ie $n_1 = k_n n_2$, where k_n denotes some scale factor, which may not be equal to k_s from equation 2.4), an amplitude control technique may be used to adjust the amplitudes and cancel out the common-mode noise. With this in mind, we can derive a new differential measurement approach, which can be described mathematically as the following. The two photodetector signals v_1 and v_2 are given by

$$v_1 = s_1 + n_1 \tag{2.8}$$

$$v_2 = s_2 + n_2 \tag{2.9}$$

The two signals v_1 and v_2 have different SNRs r_1 and r_2 respectively, with v_1 having a

higher SNR due to brighter lighting conditions (ie $r_1 > r_2$)

$$r_1 = \frac{s_1}{n_1} \tag{2.10}$$

$$r_2 = \frac{s_2}{n_2} \tag{2.11}$$

We also assume that the BVP signals s_1 and s_2 are scaled versions of each other with factor k_s

$$s_1 = k_s s_2 \tag{2.12}$$

Rearrange equations 2.10 and 2.11 for s_1 and s_2 respectively, and substitute them into equation 2.12

$$r_1 n_1 = k_s r_2 n_2 \tag{2.13}$$

Solving for n_1, we obtain

$$n_1 = \frac{k_s r_2}{r_1} n_2 = k_n n_2 \tag{2.14}$$

Therefore, we now have the following three relationships for the BVP signal, noise, and their scale factors

$$s_1 = k_s s_2 \tag{2.15}$$

$$n_1 = k_n n_2 \tag{2.16}$$

$$k_s \frac{r_2}{r_1} = k_n \implies k_s > k_n \tag{2.17}$$

2.3 The Complete Motion Artifact Cancellation Model

The previous section fully characterized the signals obtained from the two photodetectors, and also identified the need for gain/amplitude control. We will now derive the complete motion artifact cancellation model using these characterized dual channel signals.

2.3.1 Calibration and Motion Artifact Extraction

Ideally, we would like to multiply the second channel v_2 with the scale factor k_n so that we can take the following differential measurement and cancel out the noise components

$$v_d = v_1 - k_n v_2 = (s_1 + n_1) - k_n(s_2 + n_2) = (s_1 + n_1) - k_n(\frac{s_1}{k_s} + \frac{n_1}{k_n}) = (1 - \frac{k_n}{k_s})s_1 \tag{2.18}$$

However, there is no good approach to determining k_n or adjusting the gain to match the noise amplitudes, since the BVP signal components are present in the channel as well, and there is no systematic way of determining when the noise amplitudes have matched and cancelled out. It is, however, possible to adjust the gain on the v_2 channel precisely to k_s, since when there are no motion artifacts (ie when the user stays still and $n_1 = n_2 = 0$), we can adjust the gain on v_2 and calibrate until the two BVP signals cancel out to zero at gain=k_s

$$v_d = v_1 - k_s v_2 = s_1 - k_s s_2 = s_1 - k_s \frac{s_1}{k_s} = 0 \tag{2.19}$$

If we can make use of this calibration stage at the beginning to set the channel 2 gain to

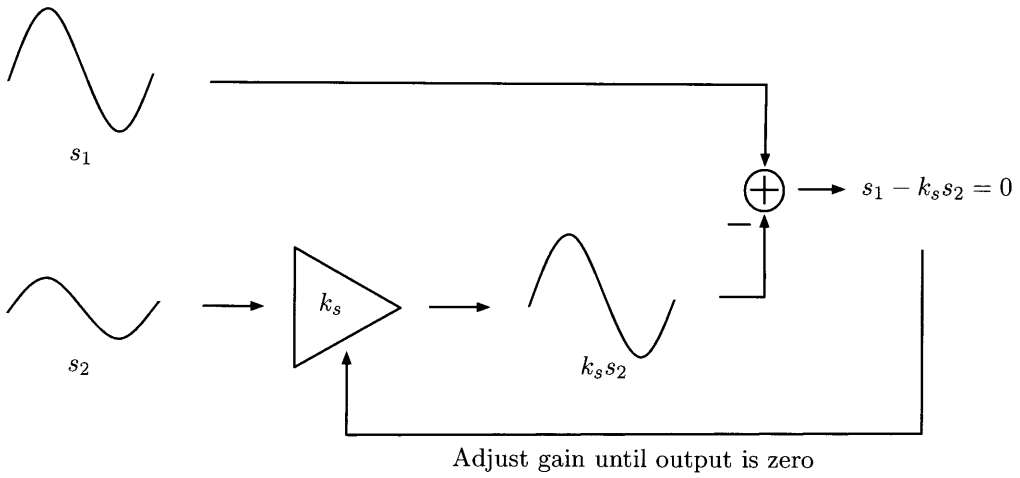

Figure 2-3: Calibration mechanism.

k_s while the user stays still, we can now extract the pure noise content from the differential measurement once the motion artifacts are added

$$v_d = v_1 - k_s v_2 = (s_1 + n_1) - k_s(s_2 + n_2) = (s_1 + n_1) - k_s(\frac{s_1}{k_s} + \frac{n_1}{k_n}) = (1 - \frac{k_s}{k_n})n_1 \tag{2.20}$$

Since we know that $k_s > k_n$, the extracted noise content is inverted. To fix the polarity, we take the differential measurement by subtracting v_1 from $k_s v_2$ instead

$$v_d = k_s v_2 - v_1 = k_s(s_2 + n_2) - (s_1 + n_1) = k_s(\frac{s_1}{k_s} + \frac{n_1}{k_n}) - (s_1 + n_1) = (\frac{k_s}{k_n} - 1)n_1 \tag{2.21}$$

The usefulness of this approach may not be obvious at first. However, the generated pure

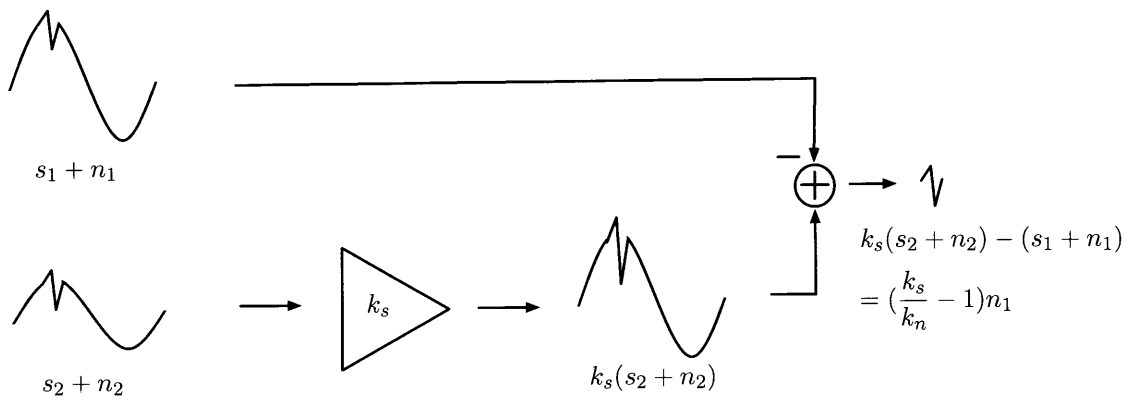

Figure 2-4: Motion artifact noise extraction.

motion artifact noise reference can now be auto gain controlled to cancel out the motion artifacts from one of the PPG channels.

2.3.2 Automatic Gain Control (AGC) and Motion Artifact Cancellation

Since we now have the pure motion artifact noise reference, we can adjust its amplitude to match the motion artifacts in the v_1 channel by using automatic gain control (AGC). An AGC system takes an input signal (in this case the noise reference) and applies a gain on this signal such that the average value of the output signal matches the provided average value reference. This is shown in the block diagram below.

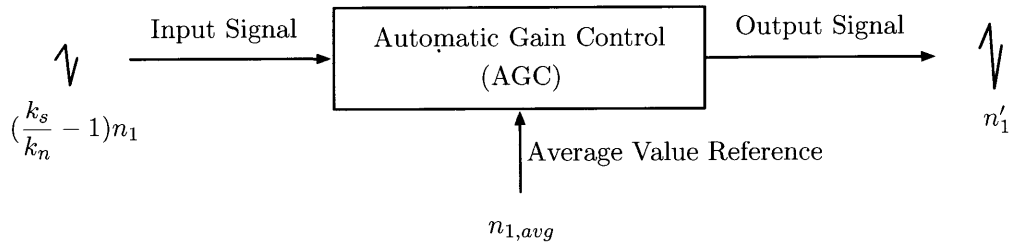

Figure 2-5: Automatic gain control.

If we can determine the average value of the motion artifact noise n_1 that is actually present in channel v_1, then we can use it as an average value reference to the AGC to adjust the noise reference amplitude to match the motion artifact n_1 in channel v_1. Mathematically, the effect of AGC can be treated as applying an adjustable gain A on the result of equation 2.21 to estimate and match the amplitude of n_1. We call this the estimated motion artifact

n_1'.

$$n_1' = (\frac{k_s}{k_n} - 1)n_1 \times A \tag{2.22}$$

In the ideal case A = $\frac{k_n}{k_s - k_n}$, the estimation n_1' matches n_1 perfectly

$$n_1' = (\frac{k_s}{k_n} - 1)n_1 \times A = (\frac{k_s}{k_n} - 1)n_1 \times \frac{k_n}{k_s - k_n} = n_1 \tag{2.23}$$

To obtain the average value reference for the noise content n_1 in channel v_1, the average value of the channel v_1 BVP signal (ie average value of s_1) can be stored during the calibration stage. Any increase in the average value of v_1 after calibration will be due to the motion artifact noise n_1 that is now added to the v_1 channel, so the difference between the average value of v_1 and the stored average value of s_1 will be the estimated average value of the noise content n_1'.

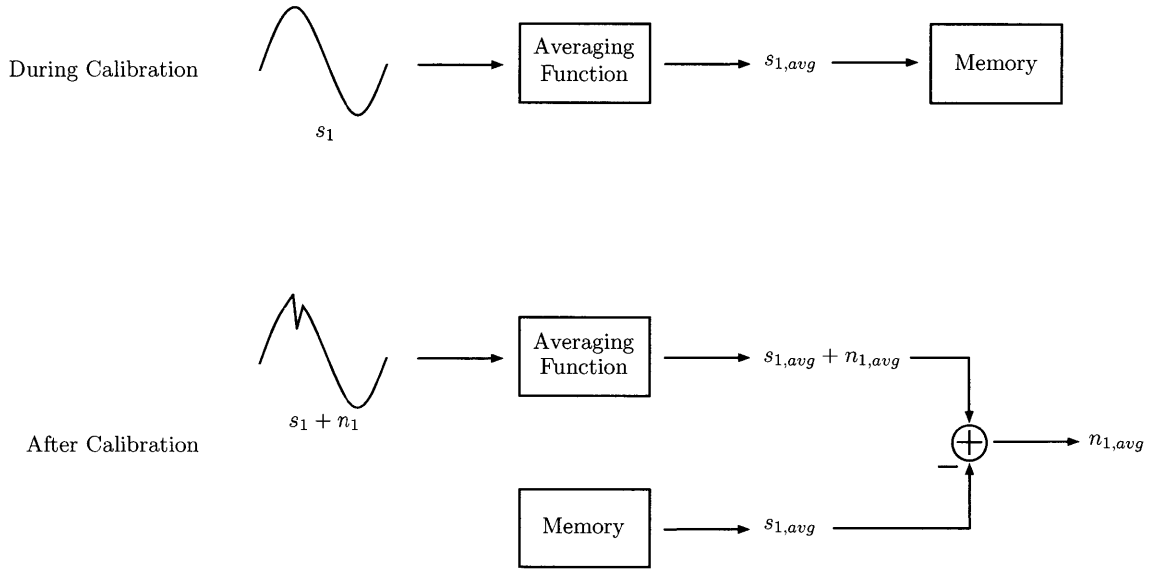

Figure 2-6: Average noise level estimation.

Once the AGC adjusts the amplitude of the noise reference, this can then be subtracted from channel v_1 to cancel out the motion artifacts and recover the original BVP signal. We call this the estimated BVP signal s_1'.

$$v_1 - n_1' = s_1 + n_1 - n_1' = s_1' \tag{2.24}$$

As the expression above shows, the recovery of the BVP signal is dependent on how well

the AGC matches the amplitude of the noise reference. In the ideal case when $n_1' = n_1$, the BVP signal is fully recovered and $s_1' = s_1$.

The complete motion artifact cancellation model block diagram is shown below.

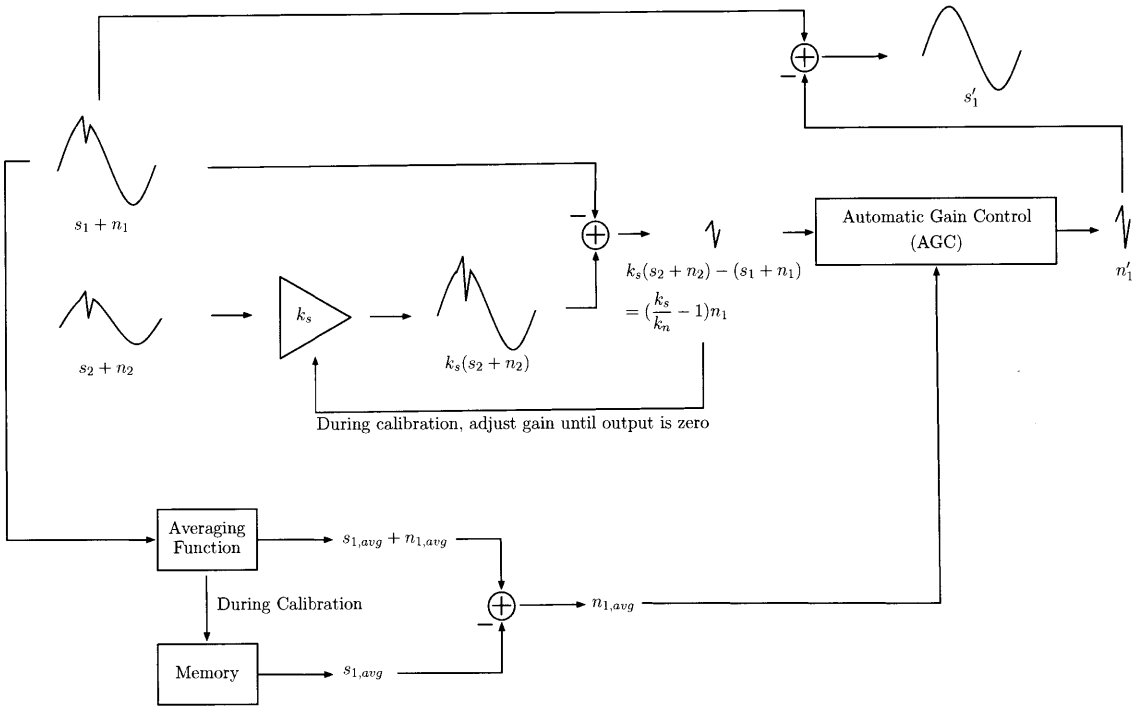

Figure 2-7: Complete motion artifact cancellation model.

Chapter 3

Design and Implementation

The previous chapter outlined the theoretical noise cancellation model for the analog front-end of a PPG sensor. This new model can potentially introduce real-time, improved performance motion artifact cancellation technique for recovering the BVP signal from a PPG channel. In order to evaluate the effectiveness of this approach, a wearable wireless wrist PPG sensor/logger was designed based on the theoretical model. This chapter describes in detail the hardware implementation of this PPG sensor.

3.1 Design Considerations

3.1.1 Power Supply Considerations

Since this is a portable, wireless wristband sensor design, it is convenient and practical to run the system on a rechargeable battery, together with a power management IC that can charge the battery using an USB port, and also be able to regulate a moderately low single-supply voltage rail. Also, since a significant portion of the hardware will be designed as analog circuitry to implement the PPG sensor front-end (and the motion artifact cancellation section, as will be discussed later), this will require a clean, minimal noise supply voltage, and it would be highly beneficial to separate the analog and the digital power rails. The analog rail should be supplied with a low noise linear regulator, and the digital rail should be supplied with a higher efficiency (but also higher ripple noise) switching regulator.

3.1.2 Motion Artifact Cancellation Implementation

The sensor will need a microcontroller on board for PPG data transmission or logging, and the motion artifact cancellation can potentially be implemented in firmware to run on the microcontroller. This will be an advantage in terms of component count and physical size of the sensor. However, the motion artifact cancellation model developed in the previous chapter is based solely on analog signal processing concepts. Therefore, the majority of the motion artifact cancellation can be, and should be, implemented in analog circuitry. This will save a significant amount of computation required on the microcontroller side, reduce complexity, and can potentially lead to lower power consumption by allowing the microcontroller to run on a slower clock or occasionally be put to sleep. The power consumption of certain commercial opamps nowadays can be on the order of micro or even nano amps, and this will be significantly lower than the power consumption of a microcontroller, which is typically on the order of 10 or 20 milliamps. There are many small, quad-pack DFN opamps available on the market, and physical size of the sensor should not be a problem if such components are used and appropriately laid out.

3.1.3 Wireless Transmission, Logging, and Other Peripherals

Our attempt is to develop a wearable wireless wristband PPG sensor, which means that the sensor must be able to either transmit the PPG data wirelessly, or log the data locally on the board. This requires a wireless transmitter (such as a Bluetooth module), and a flash-memory logger (such as a microSD card). It may also be of interest for us to connect the sensor to a USB port on a computer to transfer the data from the microSD card to the computer, as microSD card slots are not very common among most computers currently out on the market.

Also, since we are dealing with motion artifacts on the PPG signal, 3-axis motion information obtained from an accelerometer may be beneficial for insights into characterizing the performance of the sensor and also for potential troubleshooting.

3.2 System Overview

With the above design considerations taken into account, the PPG sensor system overview is shown in the figure below. The system consists of three main subsystems: power man-

agement and regulation, PPG front-end and analog motion artifact cancellation, and digital system management and peripherals. The power management and regulation system provides regulated power to the entire sensor board, with separate power rails for the digital and analog subsystems. The PPG front-end and analog motion artifact cancellation system takes the PPG signal from the user's wrist, and outputs a motion artifact cancelled, recovered BVP signal. Finally, the digital system management and peripherals section digitally manages and controls the entire sensor board, and its primary function is to sample the recovered analog BVP signal and transmit this wirelessly over Bluetooth or store onto a microSD card.

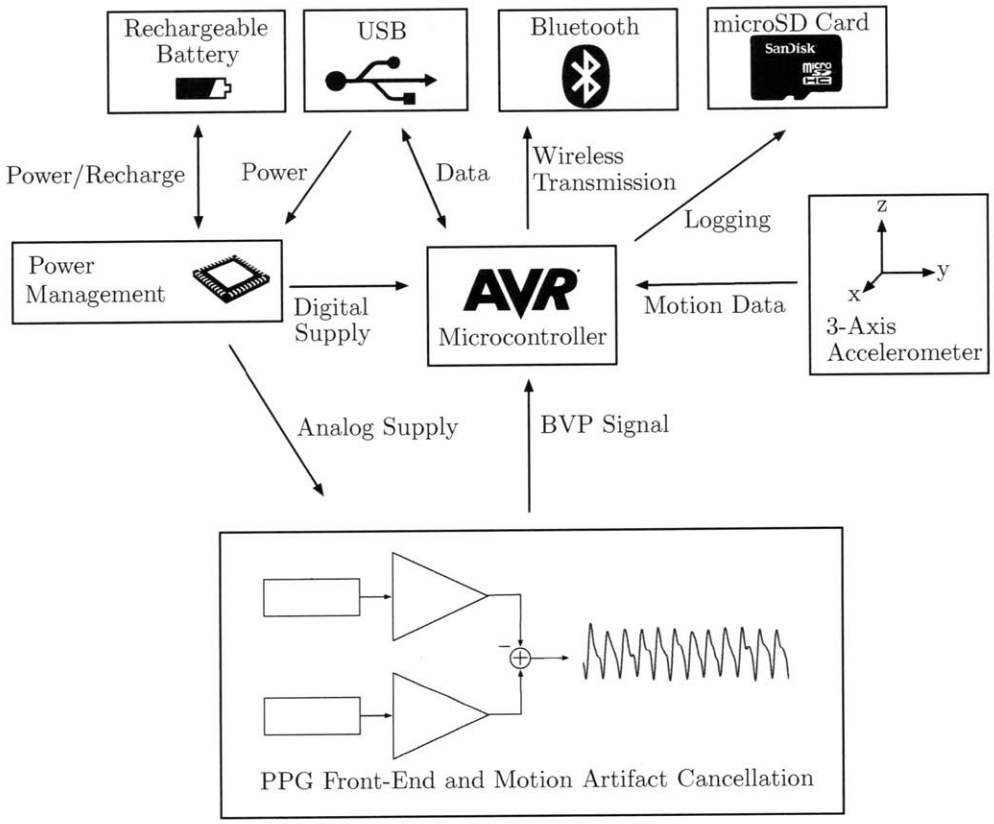

Figure 3-1: System overview.

3.3 Power Management and Regulation

This subsystem consists of three components: a micro USB connector, a lithium-ion battery, and an LTC3553 power management IC. The micro USB connector provides USB bus power

(+5V, 500mA) from a computer USB port. The lithium-ion battery is a rechargeable battery that can be used as a portable power source. The LTC3553 is a power management IC that integrates all of the functionality mentioned in section 3.1.1 in a single component. The LTC3553 can use either the USB bus power or the lithium-ion battery as its input power source, and when USB power is available, it recharges the lithium-ion battery. The IC automatically detects the available power input, and regulates the power to two outputs: a linear regulated output and a buck converted output.

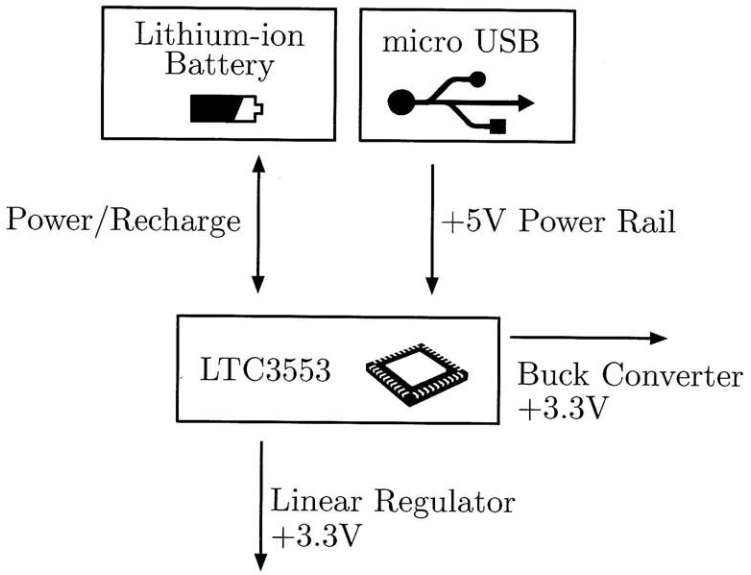

Figure 3-2: Power management and regulation.

The LTC3553 schematic is shown below. The VBUS input (the USB power bus) or the BAT input (the battery voltage) is internally tied directly to the VOUT pin, depending on which is available (if USB power is available, the system will use that instead of the battery). Therefore the voltage on VOUT is the raw voltage coming directly from either the USB power bus or the battery. This voltage is then fed into the VINLDO and BVIN pins, which are the input pins for the linear and buck regulators.

The LDO and SW pins are the linear and buck regulator output pins respectively. The regulator output voltages are determined by the feedback resistor pairs that feed back a fraction of the output voltages on LDO_FB and BUCK_FB, so that they match the internal

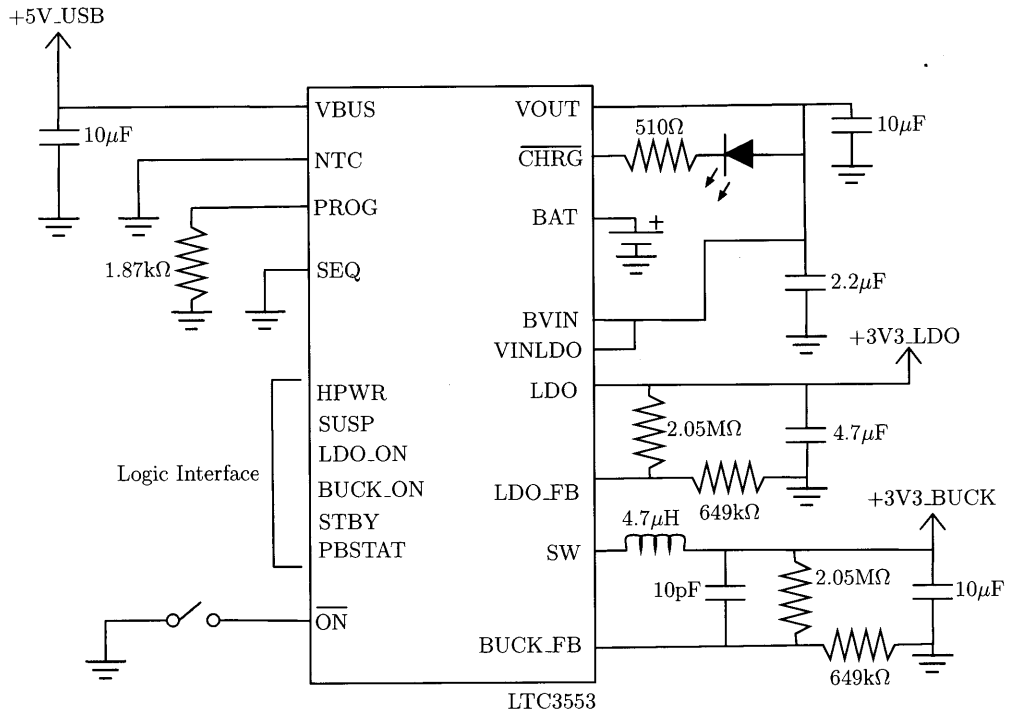

Figure 3-3: LTC3553 schematic.

reference voltage of 0.8V. Therefore the output voltage is programmed by

$$v_{out} = 0.8(\frac{R1}{R2} + 1) \tag{3.1}$$

where R1 and R2 are a feedback resistor pair that forms a potential divider on the output voltage. Since a majority of the components considered for this sensor board run on +3.3V single-supply rail, both the linear and the buck regulator outputs are configured for +3.3V, and this results in R1 = 2.05MΩ and R2 = 649kΩ.

The LTC3553 also manages the recharging of the lithium-ion battery when the USB bus power is available. The charging current is determined by the resistor on the PROG pin with the formula

$$I_{CHG} = \frac{750}{R} \tag{3.2}$$

By default, the recommended value is R = 1.87kΩ, which is approximately 400mA. The IC will automatically load balance between the regulated outputs and the charging battery to meet the USB specification of 500mA.

The LTC3553 is designed to have a logic interface that controls its regulated outputs

using digital inputs from a microcontroller. The linear and buck regulators can be turned on and off using this logic interface, and this allows us to turn off the regulator outputs with firmware control so that for example, writing to the microSD card will not be abruptly interrupted by a power cut off. The power button interface on the LTC3553 is designed as a state machine that works in conjunction with the logic from the microcontroller to allow for a safe power shutdown[1].

3.4 PPG Front-End/Analog Motion Artifact Cancellation

The block diagram of this subsystem, based on the model derived in chapter two, is shown below.

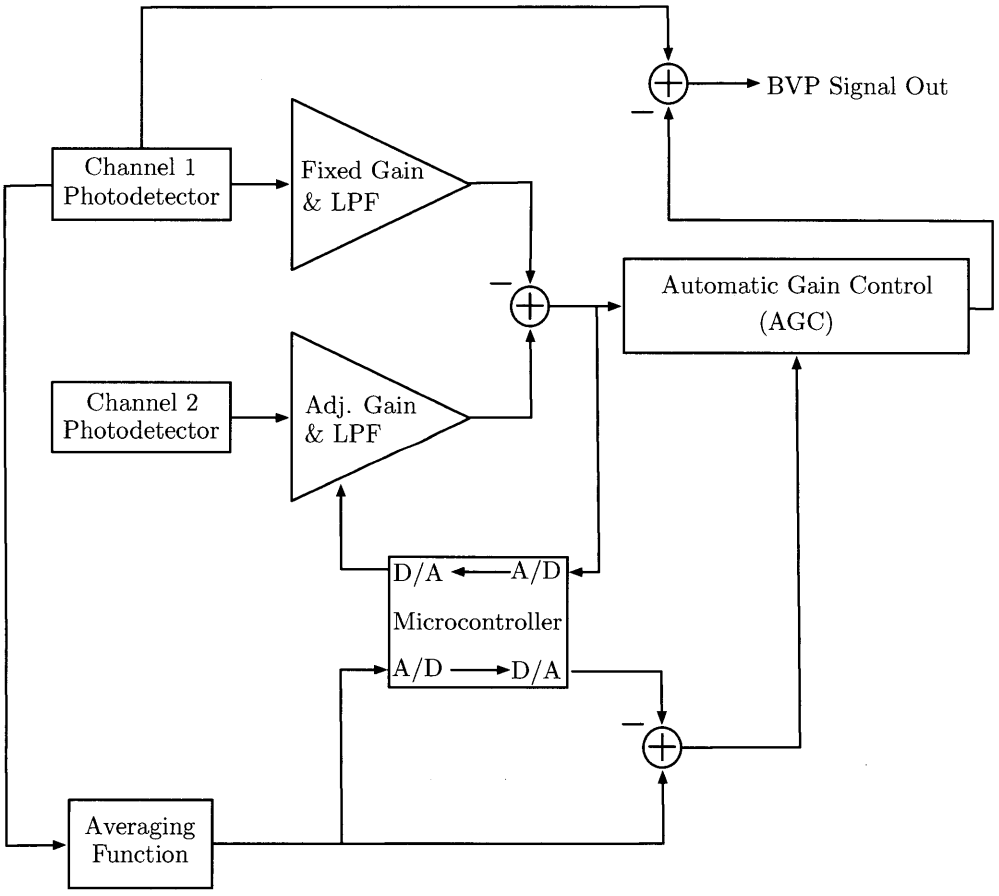

Figure 3-4: PPG front-end and analog motion artifact cancellation block diagram.

[1]For details on the state machine functionality, please refer to the LTC3553 datasheet.

3.4.1 Photodetector Input

This is the photodetector input circuit for the sensor header, which is in contact with the skin to obtain the PPG signal (the component layout is discussed in section 2.3.2). The photodetector consists of a green LED with $\lambda = 570nm$ (this particular wavelength is used to maximize the overall SNR of the PPG signal [9]), which has a nominal forward voltage of 2.1V. With a 3.3V driving rail and a 330Ω resistor in series, the driving current of the LED is approximately 3.6mA. Since there is no reasonable way to determine the optimal driving current for the LED, the series resistor can be adjusted accordingly as a compromise between SNR and power consumption.

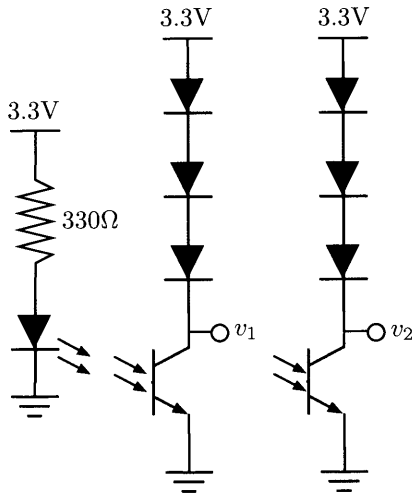

Figure 3-5: Photodetector input schematic.

The LED light is reflected off the skin and detected by the phototransistor, which has a peak sensitivity at the same wavelength of $\lambda = 570nm$. This generates a current through the phototransistor and the three diodes, which will generate a logarithmic voltage response on the output. The diodes are used instead of a load resistor to limit the output dynamic range, and they also provide a DC offset of three diode drops, which is approximately half the 3.3V supply rail (0.6V×3 = 1.8V). Having this offset gurantees the top and bottom headroom for the signal, eliminating the risk of clipping at the input stage.

3.4.2 Channel 1 Fixed Gain and Low Pass Filter

Channel 1 carries the signal from the phototransistor placed closer to the LED, which means that the SNR in this channel is higher compared to channel 2. According to our model, we apply a fixed gain on this channel to amplify the PPG signal to a suitable level. This circuit essentially consists of two cascaded gain stages each with a gain of 100, with AC coupling stages in between to remove any offset caused by the high-gain stages. Since our signal of interest is in the frequency range between 0.8Hz to 4Hz, the gain stage should also apply a low pass filter to eliminate any unwanted high frequency noise.

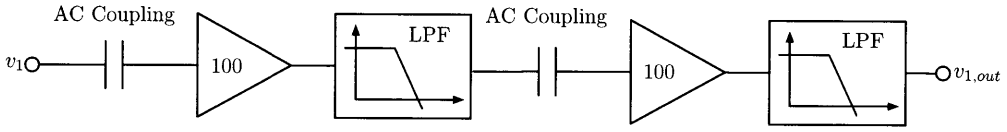

Figure 3-6: Channel 1 block diagram.

Since our design runs off of a +3.3V single-supply rail, a half supply reference is used throughout the design to offset the signal to mid rail. Generally when a gain block is built in a single-supply system, it is convenient to use an inverting amplifier topology with the non-inverting input connected to the half-rail reference. However, our system requires a high-gain stage on the order of 100, and this inherently makes the feedback resistor large. With such a large feedback resistor, in order to AC couple the input and also low-pass filter the output for the frequency range of interest (0.8Hz to 4Hz), the time constants increase significantly, and the charging of the input capacitor becomes extremely slow due to the indicated charging path. This leads to a slow build-up of the DC block voltage on the input capacitor initially when the sensor is worn, and may take a while before the AC signal actually appears in the channel.

Therefore, instead of using an inverting amplifier topology, our design uses a non-inverting amplifier in a single-supply topology, with isolated AC coupling stages. The LT1491A quad opamps are used for the amplifier implementation. As shown in the circuit diagram, the AC coupling time constant is isolated from the low pass filter stage, and the charging of the input capacitor becomes much faster. The AC coupling stages consist of a 2.2μF capacitor and a 100kΩ resistor, resulting in a cutoff frequency of approximately

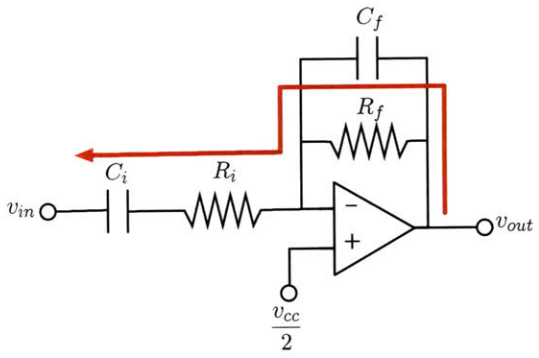

Figure 3-7: Inverting amplifier topology. The red arrow indicates the charging path of the input capacitor.

0.7Hz

$$f = \frac{1}{2\pi RC} = \frac{1}{2\pi \times 100k\Omega \times 2.2\mu F} \approx 0.7Hz \tag{3.3}$$

The non-inverting amplifier gain of each stage is set to 101 (approximately 100 gain) with a 1MΩ and 10kΩ resistor

$$A = \frac{R_1 + R_2}{R_1} = \frac{10k\Omega + 1M\Omega}{10k\Omega} = 101 \tag{3.4}$$

The 40nF capacitor in the feedback network of the non-inverting amplifier provides a low frequency cutoff, at the corner frequency

$$f = \frac{1}{2\pi RC} = \frac{1}{2\pi \times 1M\Omega \times 40nF} \approx 4Hz \tag{3.5}$$

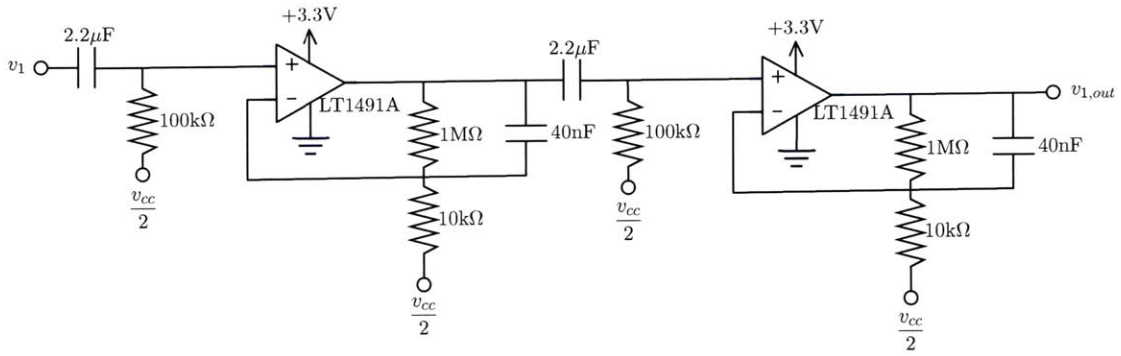

Figure 3-8: Channel 1 schematic with non-inverting amplifier.

One minor issue with this topology (that was identified after the boards were printed) is that this is not a low pass filter, but is a low frequency booster. For a high frequency signal, the capacitor in the opamp feedback path shorts, resulting in a buffer topology with a gain of 1. Therefore, the circuit applies a gain of 101 on the low frequencies, but maintains the high frequencies with unity gain and does not attenuate them. This is not a major issue since there are no large amplitude high frequency components entering the system. However in the future, it may be beneficial to add an RC low pass filter stage on the input to provide attenuation on the higher frequencies as well.

3.4.3 Channel 2 Adjustable Gain and Low Pass Filter

Channel 2 carries the signal from the phototransistor placed further away from the LED, resulting in a lower SNR compared to channel 1. The basic topology of this system is identical to the channel 1 fixed gain case. However, since the gain of this channel must be adjustable, an LM13700 operational transconductance amplifier (OTA) is added in between the two gain stages to provide a voltage controlled gain stage.

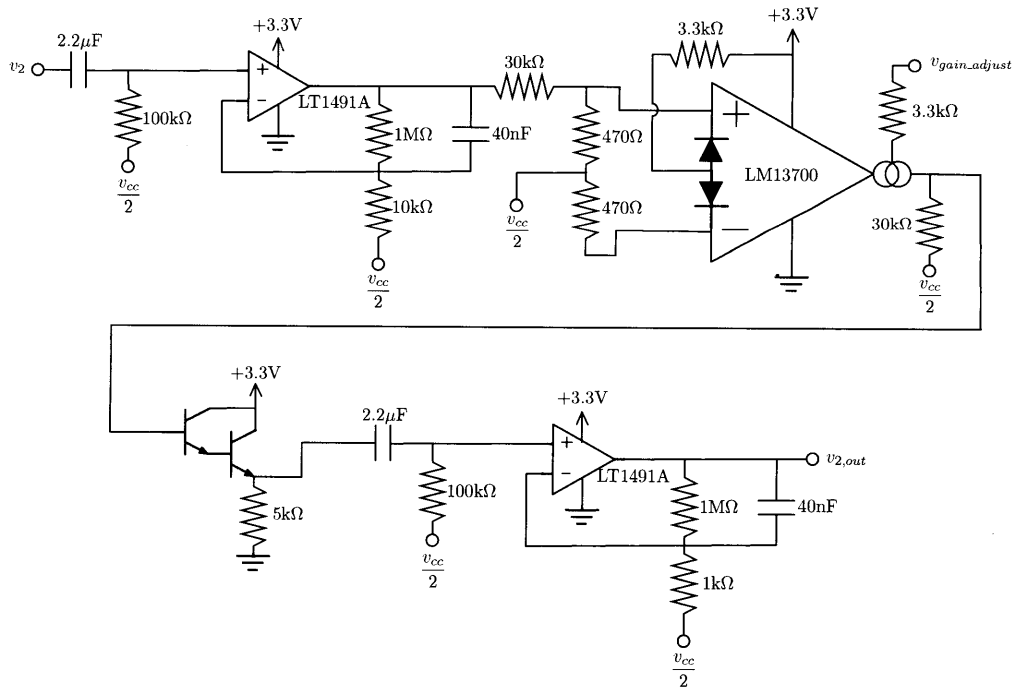

Figure 3-9: Channel 2 schematic.

To maintain linearity and minimize distortion, the OTA is configured for an adjustable

gain between 0 to 1. Since the gain range of this channel needs to be adjustable to match the BVP signal amplitudes of the two channels, we would like some margin above and below the channel 1 gain. Therefore the second fixed gain stage in channel 2 is configured to be 1001, with a 1kΩ resistor in the feedback path instead of a 10kΩ resistor. While channel 1 has a fixed gain of approximately $100\times100 = 10^4$, channel 2 has an adjustable gain between 0 and $100\times1\times1000 = 10^5$. The gain adjustment is controlled by the DAC voltage output from the microcontroller.

3.4.4 Instrumentation Amplifier Stage for Motion Artifact Extraction

This is an AD8226 instrumentation amplifier stage used to take the difference between channel 2 and channel 1. The inamp is configured to have unity gain, and is also referenced at mid rail. During calibration, the output of this inamp is read by an ADC channel on the microcontroller, and the microcontroller adjusts the DAC voltage to the OTA to adjust the channel 2 gain and match the BVP signal amplitudes in the two channels until the inamp output contains no BVP signal. Once this point is reached, the microcontroller maintains the DAC voltage to the OTA to fix the channel 2 gain, and any signal output from the inamp from this point on will only contain motion artifacts.

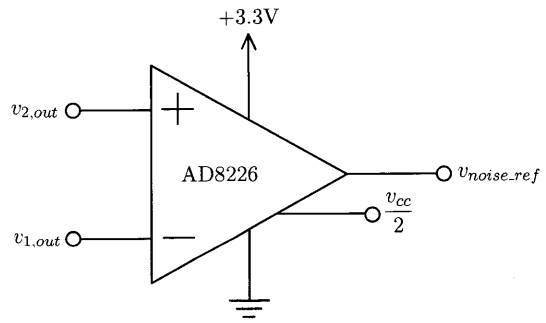

Figure 3-10: Motion artifact extraction stage.

3.4.5 Average Motion Artifact Noise Estimation

During calibration, the average level of the BVP signal in channel 1 is determined and stored to estimate the average noise level present in channel 1 when motion artifacts are added. The average level of the signal is generated by full-wave rectifying the signal and applying a low pass filter to average out the rectified signal. Both the full-wave rectifier and the low

pass filter are implemented as discrete designs using the LT1491A quad opamps. The low pass filter is a second order sallen-key topology, and this is used to provide a sharp cutoff frequency at a frequency much lower than 0.8Hz, to eliminate any ripple in the average value and provide a stable average reference. The cutoff frequency is given by

$$f = \frac{1}{2\pi R^2 C^2} = \frac{1}{2\pi \times (300k\Omega)^2 \times (4.7\mu F)^2} \approx 0.08Hz \tag{3.6}$$

The cutoff frequency is a decade below 0.8Hz, and with this second order filter, the double pole roll-off will provide an attenuation of 40dB.

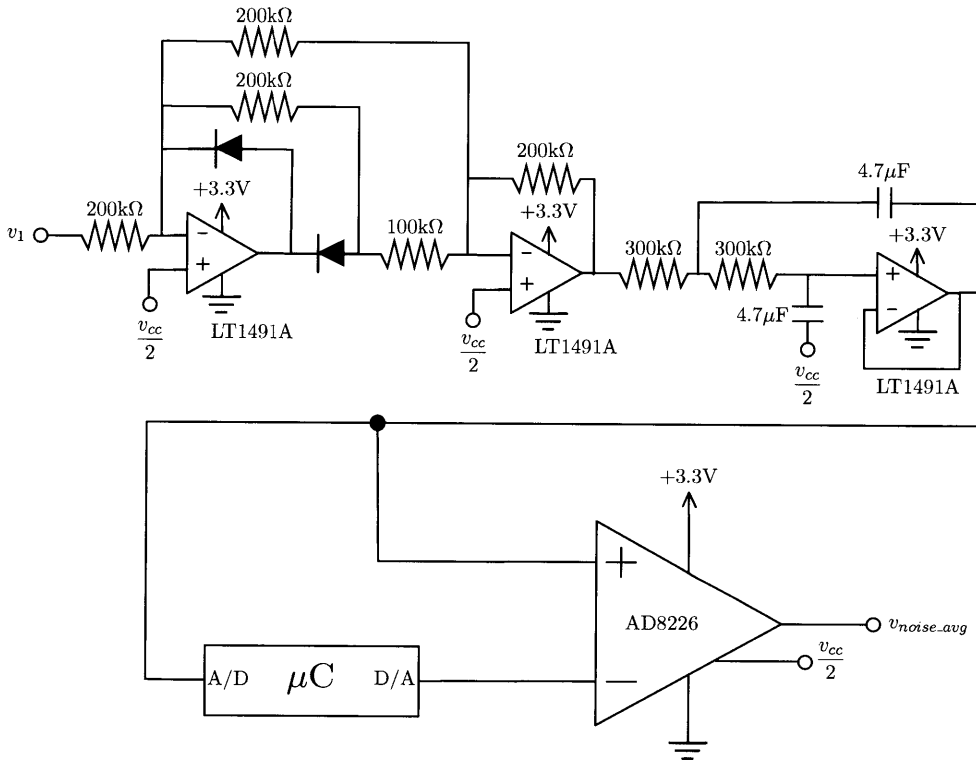

Figure 3-11: Channel 2 schematic.

During calibration, the microcontroller reads and stores the average value of the channel 1 BVP signal from the low pass filter output using one of the ADC channels. Once the calibration is completed, the microcontroller outputs the stored average value out of the DAC, which is connected to the inverting input of another AD8226 inamp. The non-inverting input of the inamp is connected to the output of the low pass filter, which now outputs the average value of BVP signal and the motion artifact noise. Therefore the output

of the inamp will be the estimated average value of the motion artifact noise content present in channel 1.

3.4.6 Automatic Gain Control (AGC)

The AGC is probably the most complex section of this entire sensor system, and will require some detailed explanation into how the circuit operates. Various topologies have been considered for this design, but only one approach is described in this section[2].

We have the motion artifact noise signal extracted in section 3.4.4, and its average value estimated in section 3.4.5. These two outputs can now be used in the automatic gain controller to match the average value of the motion artifact signal to the estimated average value reference.

An automatic gain controller consists of three main blocks: a variable gain block, a full-wave rectifying block, and a low pass filtering block. A signal goes through the variable gain block, and the output signal is full-wave rectified and low pass filtered to compute its average value. This average value is compared to a reference value, and the variable gain is adjusted accordingly to match the output average value to the reference.

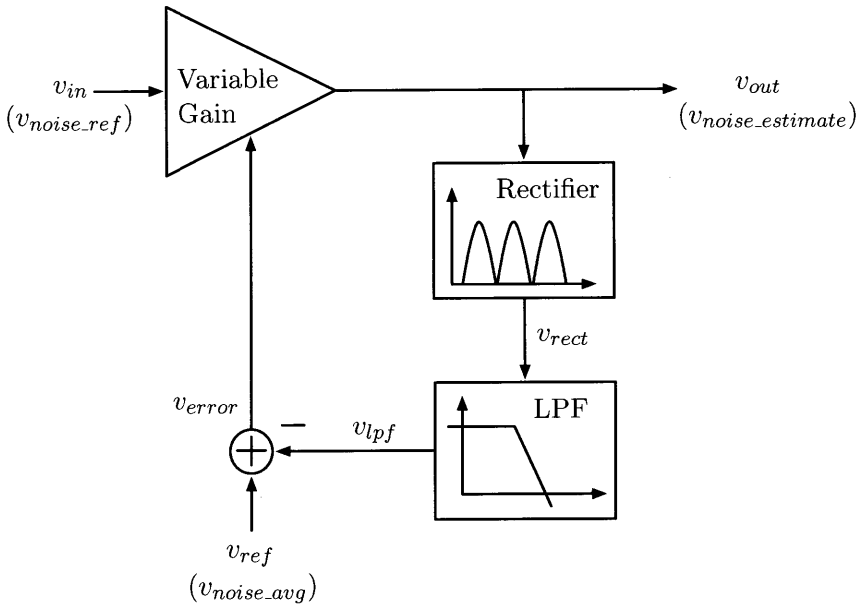

Figure 3-12: Automatic gain control block diagram.

[2]Please refer to Appendix B "Alternative Automatic Gain Control Approaches" for alternative designs.

This is essentially a controls problem, where we would like to apply feedback control to regulate the amplitude of our estimated noise signal. Therefore the parameters we are interested in include stability, bandwidth, transient response, and steady-state error.

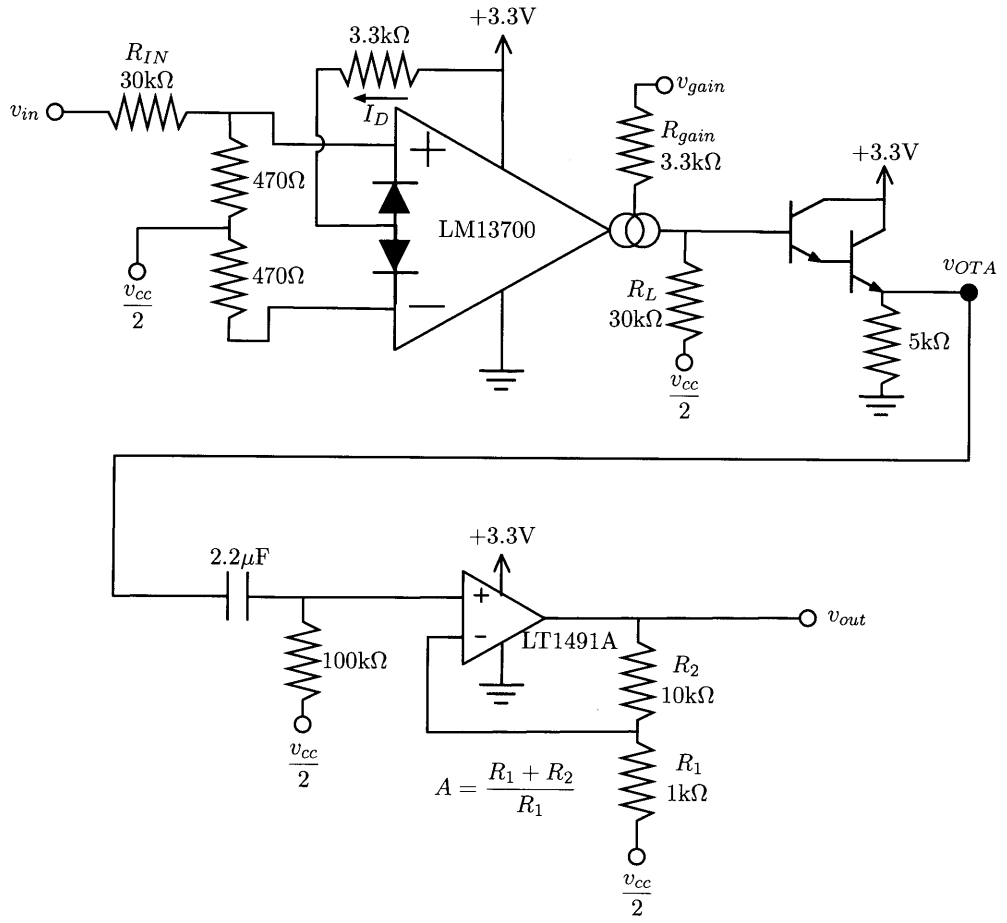

Figure 3-13: Variable gain block.

We will first look at the variable gain block in the forward path. The design of this block is similar to the adjustable gain block in section 3.4.3, where an LM13700 OTA based voltage controlled variable gain stage is followed by a fixed gain stage. The OTA configuration is identical to the topology in section 3.4.3, and the relationship between its output voltage v_{OTA} and the gain control voltage v_{gain} is given by

$$\frac{v_{OTA}}{v_{gain}} = \frac{R_L v_{in}}{R_{gain} R_{IN} I_D} \tag{3.7}$$

where v_{in} is the motion artifact signal extracted in section 3.4.4. With the fixed gain A

applied to the OTA output, the transfer function between the gain control voltage and the AGC output is

$$\frac{v_{out}}{v_{gain}} = \frac{R_L v_{in} A}{R_{gain} R_{IN} I_D} \tag{3.8}$$

In reality, the fixed gain opamp would also have a pole at around 100kHz. However, since our dominant pole will be below 1Hz due to the low pass filter stage, the opamp pole will not affect the dynamics of the system and will therefore not be considered in the analysis.

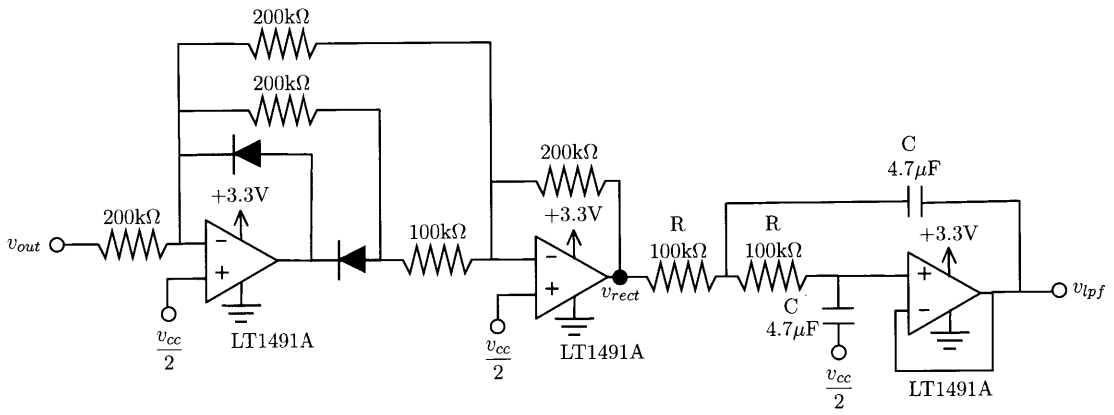

Figure 3-14: AGC feed back path with a full-wave rectifier and a low pass filter.

Now the output signal is then fed back through a full-wave rectifier and a low pass filter to convert the signal to its average value. Again, this block is very similar to the circuit designed in section 3.4.5. The full-wave rectification is a non-linear operation, and it would add some complexity to our analysis if we were to fully characterize this system. However, since our system is dominated by the characteristics of the low pass filter, the rectifier characteristics will not affect the system dynamics significantly and can be safely ignored.

The low pass filter is again a sallen-key topology filter with a double pole roll-off for a sharp, second order cutoff. From a system stability point of view, this is the highest order filter that we can afford to include in the feedback loop. Therefore, this provides the sharpest possible transition band, given that the system needs to maintain stability. Since the bandwidth of the low pass filter has a significant impact on the overall bandwidth of the system, this sharp transition band allows us to push the cutoff frequency as high as possible, while still attenuating the ripple present in the rectified output. The transfer function of

this second order filter is given by

$$\frac{v_{lpf}}{v_{rect}} = \frac{1}{R^2C^2s^2 + 2RCs + 1} \tag{3.9}$$

Since the low pass filter must cutoff at a frequency lower than the frequency range of interest (0.8Hz to 4Hz) in order to eliminate the ripple and generate the average value, the drawback of this system is that its response will be slower than the input signal. This means that the AGC system will reach its steady-state if the motion artifact is sustained, but if the motion artifact consists of short transients, the system response may not catch up on time to reach the steady-state. This is an inherent weakness in AGC systems, as the feedback of the average signal level is required. However, this is still a potentially effective approach, since motion artifacts (especially wrist motion artifacts) may occur in a sustained manner during our daily activities (eg. typing on a keyboard, swinging arms while walking, etc).

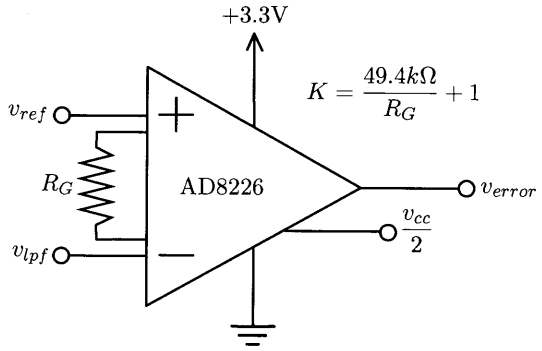

Figure 3-15: AGC subtraction junction.

Finally, the subtraction junction is implemented using an AD8226 inamp to output the error between the reference average value and the actual average value. The configurable gain feature on the inamp (configured using the gain resistor R_G) can also be used as a proportional compensator K on the error signal.

The block diagram in the figure illustrates the network of all of the mentioned transfer functions in a feedback topology. The loop transfer function of this system is given by

$$L(s) = \frac{KR_Lv_{in}A}{R_{gain}R_{IN}I_D(R^2C^2s^2 + 2RCs + 1)} \tag{3.10}$$

Using the loop transfer function, we can obtain the bode plot and the step response to

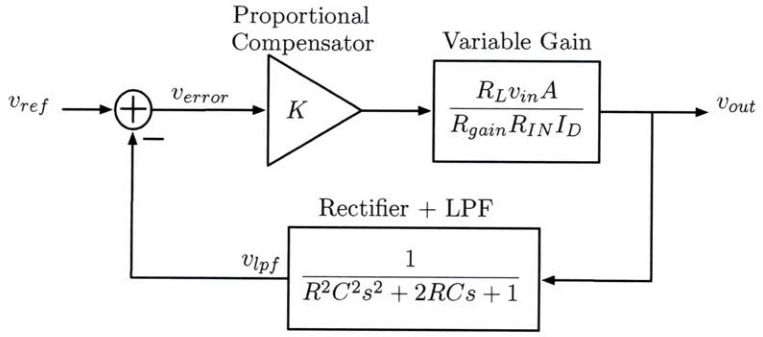

Figure 3-16: AGC feedback topology block diagram.

illustrate the performance of this closed loop system, with the compensator gain initially set to K=1.

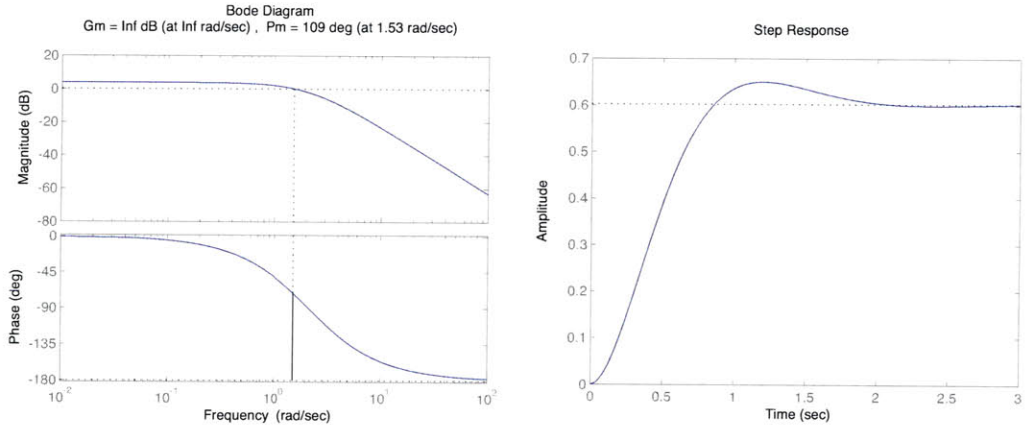

Figure 3-17: AGC loop dynamics with no compensation.

The system is clearly stable, with a phase margin of 109°. However, it suffers from a significant steady-state error (settling at approximately 60% of reference input), and the transient takes about 3 seconds to settle. The steady-state error must be improved, as amplitude accuracy is essential for the motion artifact cancellation to perform well. The error transfer function is given by

$$\frac{E}{v_{ref}}(s) = \frac{1}{1 + L(s)} = \frac{R_{gain} R_{IN} I_D (R^2C^2s^2 + 2RCs + 1)}{R_{gain} R_{IN} I_D (R^2C^2s^2 + 2RCs + 1) + K R_L v_{in} A} \tag{3.11}$$

Using the final value theorem, we obtain the steady state error

$$e_{ss} = \lim_{s \to 0} sE(s) = \frac{R_{gain} R_{IN} I_D}{R_{gain} R_{IN} I_D + K R_L v_{in} A} \tag{3.12}$$

As the expression shows, the steady-state error can be minimized by increasing the compensator gain K. Ideally, we would like to set K as high as possible so that $e_{ss} \to 0$. However, increasing K will also push the crossover frequency higher, resulting in a decreased phase margin and lower stability. Therefore, it is necessary to increase K such that it reduces the steady-state error to a suitable level (say less than 5mV), and design a compensator to increase the phase margin and restore stability.

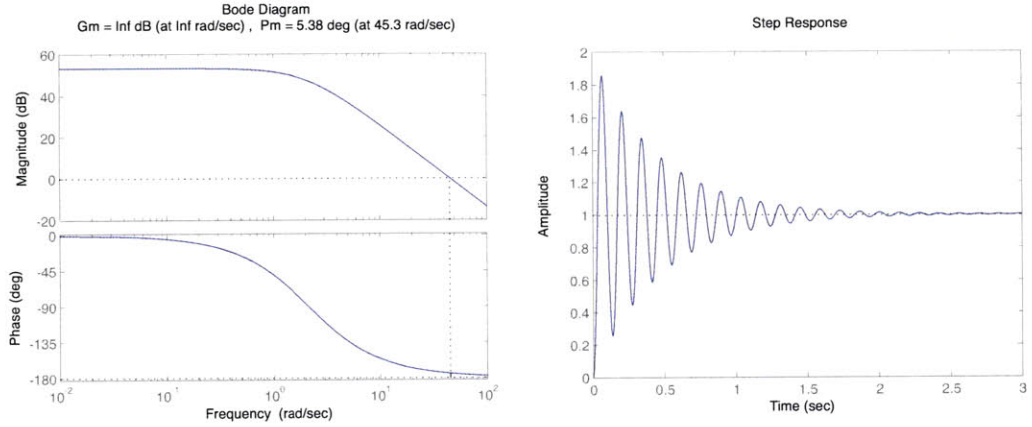

Figure 3-18: AGC loop dynamics with K=300.

Simulating in MATLAB, K=300 would reduce the steady-state error to approximately 3mV. The steady-state error is now acceptable, but the phase margin is now too small (5.38°) and the oscillation in the transient response is clearly undesirable.

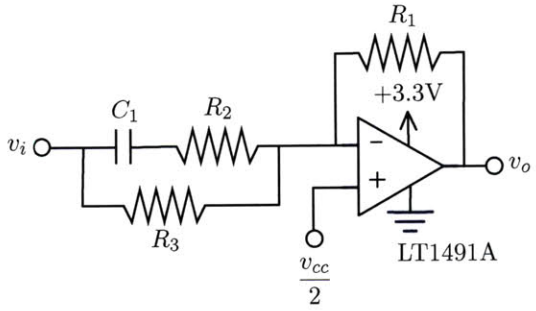

Figure 3-19: Lead Compensator.

We can design a lead compensator to provide a phase bump at the crossover frequency to recover the stability. The topology in the figure is an opamp implementation of a lead compensator, and its transfer function is given by

$$\frac{v_o}{v_i} = -\frac{R_1}{R_3}\frac{(R_2+R_3)C_1 s + 1}{R_2 C_1 s + 1} \tag{3.13}$$

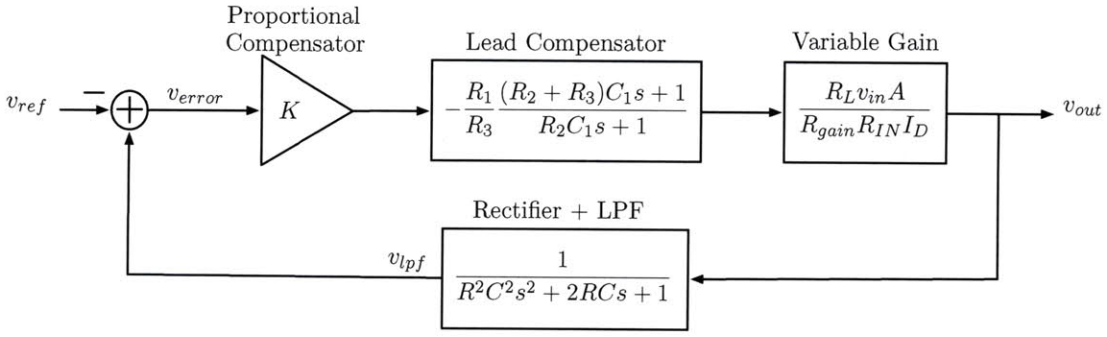

Figure 3-20: AGC feedback topology block diagram with lead compensation.

We place this compensator as shown in the block diagram above. The polarity on the subtraction junction is now switched to account for the negative sign on the compensator and to maintain negative feedback. Placing the pole-zero pair a decade apart, and with some fine tuning in MATLAB, the component values are $R_1 = 8.2k\Omega$, $R_2 = 1k\Omega$, $R_3 = 8.2k\Omega$, and $C_1 = 4.7\mu F$. The resulting plots indicate a phase margin of 55.8°, 3mV steady-state

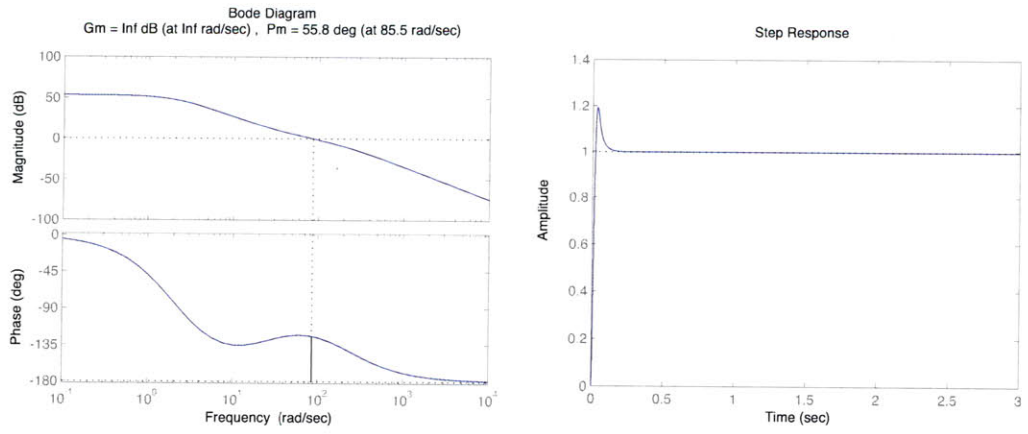

Figure 3-21: AGC loop dynamics with lead compensation.

error, and also an improved response time of approximately 0.2s. There is still some amount of peak overshoot, but the fast settling time should make the effect of the peak overshoot insignificant.

3.4.7 Motion Artifact Cancellation

Finally, the amplitude controlled motion artifact signal produced by the automatic gain control stage is subtracted from the channel 1 signal using an AD8226 inamp to cancel out the motion artifacts and recover the BVP signal. The output of this inamp is sampled by the microcontroller ADC.

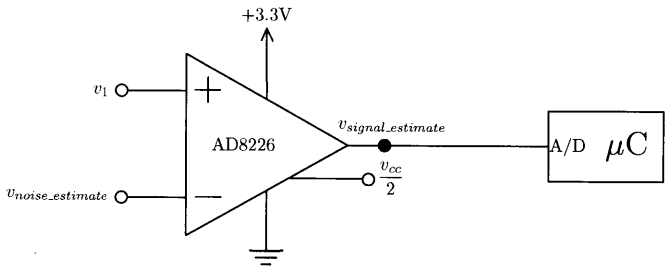

Figure 3-22: Motion artifact cancellation.

3.4.8 Half-Supply Voltage Reference

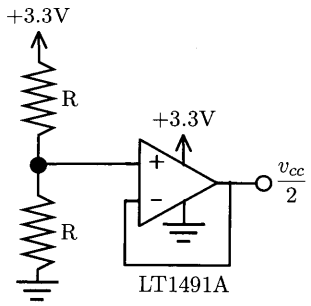

Figure 3-23: Half-supply voltage reference.

Throughout the analog section of the sensor board, a half-supply voltage reference is used for single-supply operation. This is simply a voltage divider followed by an opamp buffer. Two of these references are used to supply the entire analog section, as one reference may not have the sufficient output current capabilities to maintain a stable reference. Since

the automatic gain control section is susceptable to high frequency noise due to the lead compensator network, one reference is dedicated to this section and the other reference is used for the rest of the board.

3.5 Digital System Management and Peripherals

The final subsystem of the sensor board consists of digital components and peripherals. This includes the microcontroller, which manages and controls the entire sensor system. The block diagram of this subsystem is shown below.

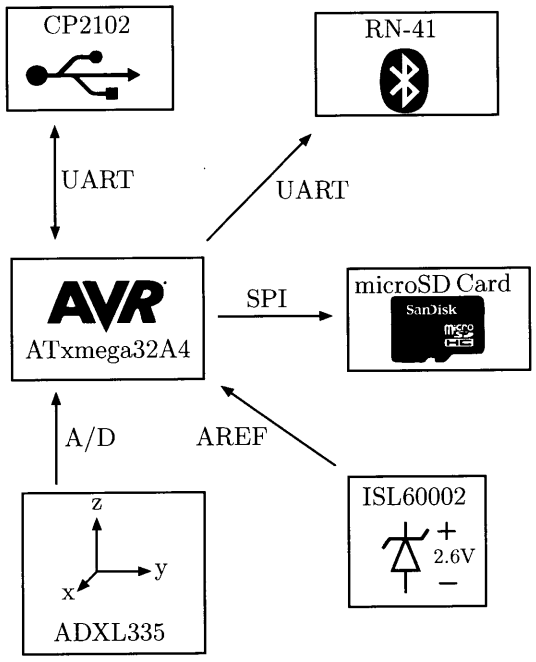

Figure 3-24: Digital system management and peripherals block diagram.

3.5.1 ATxmega32A4 Microcontroller

The microcontroller is an Atmel ATxmega32A4, which is a 44-pin component with 2 DAC channels and 12 ADC channels. The maximum reference voltage for both the DAC and the ADC is 0.6V below the supply voltage, and therefore an external analog voltage reference of 2.6V is used. The microcontroller runs on an internal clock of 32MHz, but an external clock of 14.7456MHz can also be used if high UART accuracy is desired. All of the peripherals and the analog outputs are connected to this microcontroller using various protocols and

ADC channels, and hence the microcontroller can be programmed to digitally manage and control the entire system.

3.5.2 ISL60002 Precision Analog Reference

The Intersil ISL60002 is a precision 2.6V analog reference used for the DAC and ADC on the microcontroller. The filtering layout is as recommended on the datasheet.

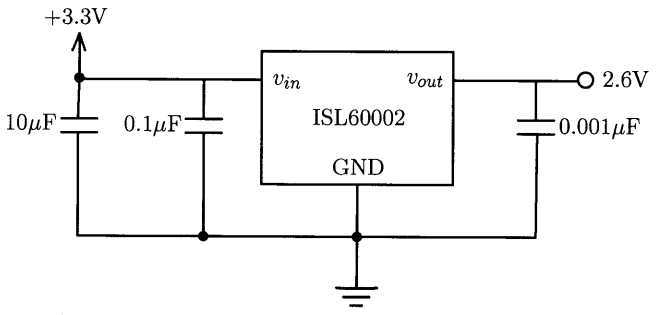

Figure 3-25: ISL60002 precision 2.6V analog reference.

3.5.3 microSD Card

The microSD card is used to log and store the sampled PPG signal. The data is written to the card from the microcontroller via SPI.

3.5.4 RN-41 Bluetooth Module

The RN-41 is a bluetooth module manufactured by Roving Networks. Data can be transferred from the microcontroller to this module via UART, and the module will transmit this data over bluetooth to other bluetooth enabled computers and cellphones. This module can be configured to be either master or slave, and in slave mode, nearby computers and cellphones can discover the module and pair with it to open a bluetooth COM port using the Serial Port Profile (SPP).

3.5.5 ADXL335 Accelerometer

The ADXL335 is a 3-axis, ±3g accelerometer that outputs analog voltages for the x, y, and z axes. The $0.47\mu F$ capacitors on each of the 3-axis outputs are placed to filter the signals and limit their bandwidth to 10Hz.

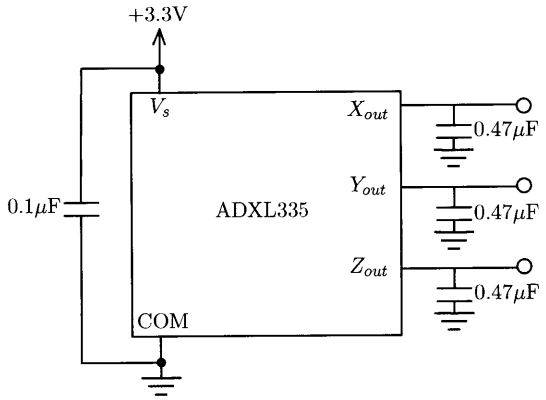

Figure 3-26: ADXL335 schematic.

3.5.6 CP2102 USB-to-UART Bridge

The Silicon Labs CP2102 chip converts the USB data lines to UART, so that the microcontroller can be interfaced to transfer data through the USB cable.

Chapter 4

Testing and Evaluation

The design outlined in the previous chapter was implemented as a wristband sensor to examine the effectiveness of the motion artifact cancellation model. This chapter describes the testing procedure and the resulting performance, together with the discussion of the issues that were encountered.

4.1 Testing Procedure and Setup

The constructed sensor board was mounted on a wristband as shown in the figure. The majority of the circuit board (together with the battery) was contained inside the wristband, and the photodetector front-end was exposed to be in contact with the skin. Firmware was written for the microcontroller for auto-calibration, where the gain of channel 2 is increased a step at a time until the BVP amplitudes of the two channels matched and cancelled out. The duration of the calibration stage was typically on the order of 20-30 seconds.

Figure 4-1: Constructed wristband PPG sensor.

The sensor board functioned as intended, except for the automatic gain control loop. There were two main issues with the AGC loop: slow transient response and high-frequency noise. The slow transient response is shown in the figure. The black line indicates the step input, and the red line indicates its response. The shape of the response matches our prediction, where the output settles with no significant oscillation. However, unlike the simulated settling time of 0.2 seconds, the actual settling time is approximately 2 seconds (each major division is 1s).

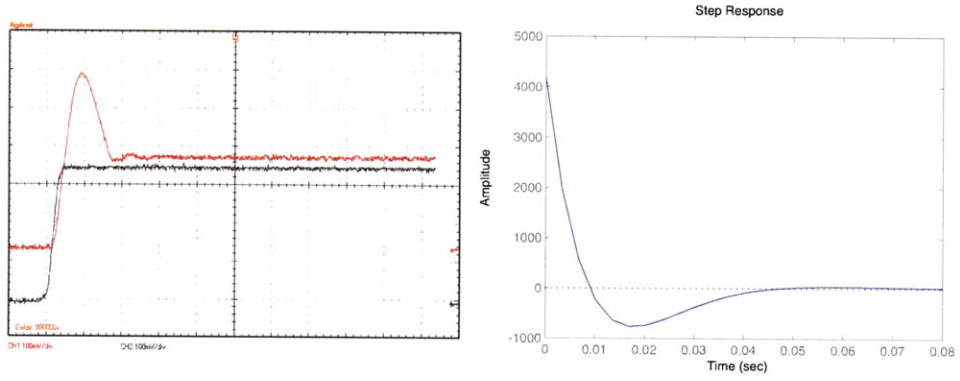

Figure 4-2: AGC slow transient response (left) and transient voltage swing of the low-pass filter input (right).

The slow transient response is due to the limitation of the power supply rail at 3.3V. In the design phase of this system, the dynamics of all node voltages were not taken into account. In order to force the low-pass filter in the feedback loop to change fast enough, its input must temporarily be pushed up to a few thousand times greater than the reference voltage change (ie few thousand volts), which is not feasible. This is a limitation due to the analog implementation, and this would not have been an issue in the digital domain where the control signals can be arbitrarily large. Therefore, in this analog approach to this problem, there are no practical solutions to increasing the speed of the transient response.

As for the high-frequency noise, the high-frequency gain introduced by the lead compensator amplifies the high-frequency edges that remain from the full-wave rectifier stage, and the resulting noise is coupled into the estimated motion artifact signal. Although the step response of the control voltages appear clean, this is due to the fact that the control voltages are strongly low-pass filtered, essentially providing an averaged version of the motion artifact signal. The actual motion artifact signal is corrupted with the noise from the lead

compensator. Again, this is a difficult problem with no practical solution, as the rectified edges cannot be attenuated further unless the low-pass filter cuts off at a lower frequency, which will result in a even slower transient response.

Therefore, instead of using a compensator, the loop was reduced back to the uncompensated system. Since our lead-compensated system has a settling time of 2 seconds, there is no significant loss in performance by switching to the uncompensated system, which also has a response time of approximately 2 seconds. The drawback, however, is in the steady-state error. The compensated system was originally designed to eliminate the steady-state error present in the uncompensated system, which was approximately 40%. This steady-state error can instead be compensated for in firmware, by offsetting the average reference input to the AGC. Since the steady-state error varies depending on the reference input level, the offset must be scaled accordingly to compensate for the changing error levels.

With the above changes implemented, the sensor was tested for various motion artifact inducing movements. The sensor was setup to transmit the PPG signal wirelessly to a computer over bluetooth, where the waveforms were displayed and logged using a processing script. Initially, the sensor was worn on the wrist for at least one minute to allow for the signal to settle and produce a clear, strong BVP pulse. Once this signal was present, the microcontroller was initiated to run the auto-calibration stage while the user remained still. After the auto-calibration stage was completed and the BVP signal amplitudes were matched, controlled movements such as gripping and swinging were conducted to evaluate the effects of the motion artifact cancellation system. While one hand is being used to evaluate the wristband sensor, a reference BVP signal was also collected from the other hand using a FlexComp BVP sensor.

In addition, the performance of the sensor as an around-the-clock logger was evaluated by collecting the sensor data over a few hours during normal day-to-day activities. The collected data was stored locally on a microSD card, and was later processed in MATLAB for peak detection, R-R interval calculation, and heart rate computation. The 3-axis accelerometer data was also collected. In order to evaluate the accuracy of the wristband sensor, the Alive sensor was used to collect ECG data as a gold standard reference.

4.2 Results and Discussion

The sensor was initially tested for sustained movements, such as continuous swinging and gripping motion. The figure shows the waveform collected from the swinging case. The first waveform is the original PPG signal coming straight from channel 1, which starts to become corrupted with the swinging motion after 3 seconds. The second waveform is the estimated motion artifact that is differentially extracted from the two channels and passed through the AGC. The third waveform is the recovered BVP signal, which is the result of the second waveform being subtracted from the first waveform. Finally, the fourth waveform is the reference BVP (ie the gold standard) obtained from the FlexComp sensor. The red dots indicate the correct pulse locations according to the FlexComp data.

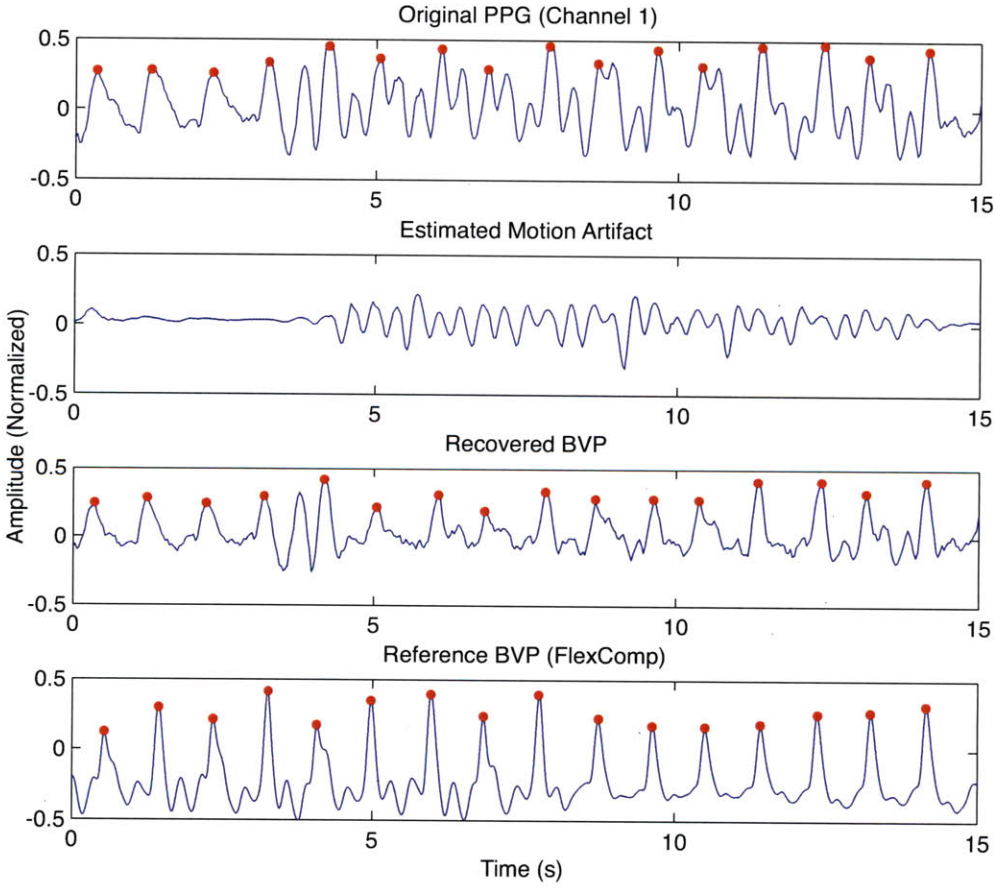

Figure 4-3: Motion artifact cancellation during swinging motion.

As shown on the plots above, the wristband sensor manages to recover the BVP pulse well when the motion is sustained for longer than 2 seconds. In the first 3 seconds, there

are no motion artifacts present in the original signal, and the sensor outputs a clear BVP signal that matches the reference BVP from FlexComp. At t=3s, the motion artifacts start to appear in the original signal, and the AGC begins to track the motion artifact present in the original signal and a waveform appears on the estimated motion artifact signal. At t=5s (ie 2 seconds after the motion artifacts appear and once the AGC catches up), the estimated motion artifact signal tracks the actual motion artifact accurately, and the BVP signal is recovered with the motion artifact ripple removed. The peaks of the recovered BVP signal match the reference BVP accurately.

Here is another set of waveforms for the continuous gripping case. Again, after the motion artifacts are added to the BVP signal, the AGC catches up after a 2 seconds delay and the motion artifact ripple is cancelled out to generate clean, well-defined BVP peaks.

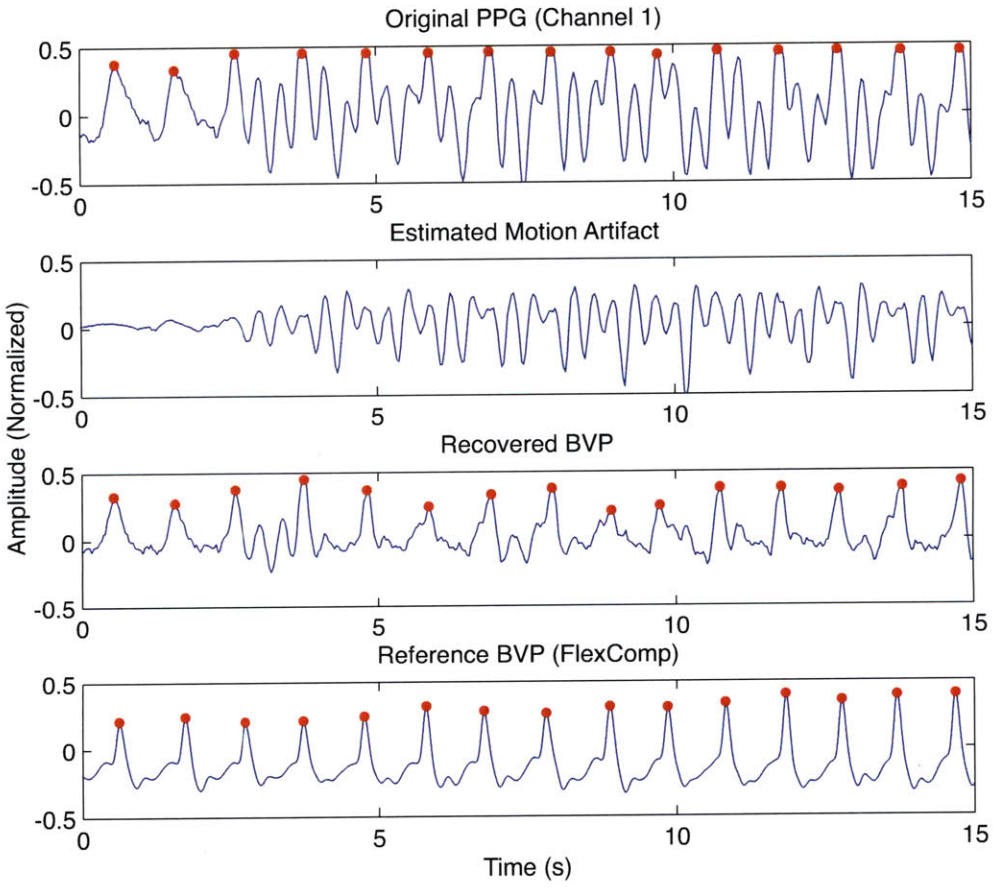

Figure 4-4: Motion artifact cancellation during gripping motion.

The sensor was then tested for a short, transient motion that lasted for less than 2 seconds. The figure below shows the waveforms obtained from a single grip case. As shown

in the original PPG signal, the motion artifacts last for approximately 2 seconds. However, the estimated motion artifact signal does not track the motion artifact due to the slow transient in the AGC loop, and the system cannot catch up and the motion artifact ripple is not cancelled out.

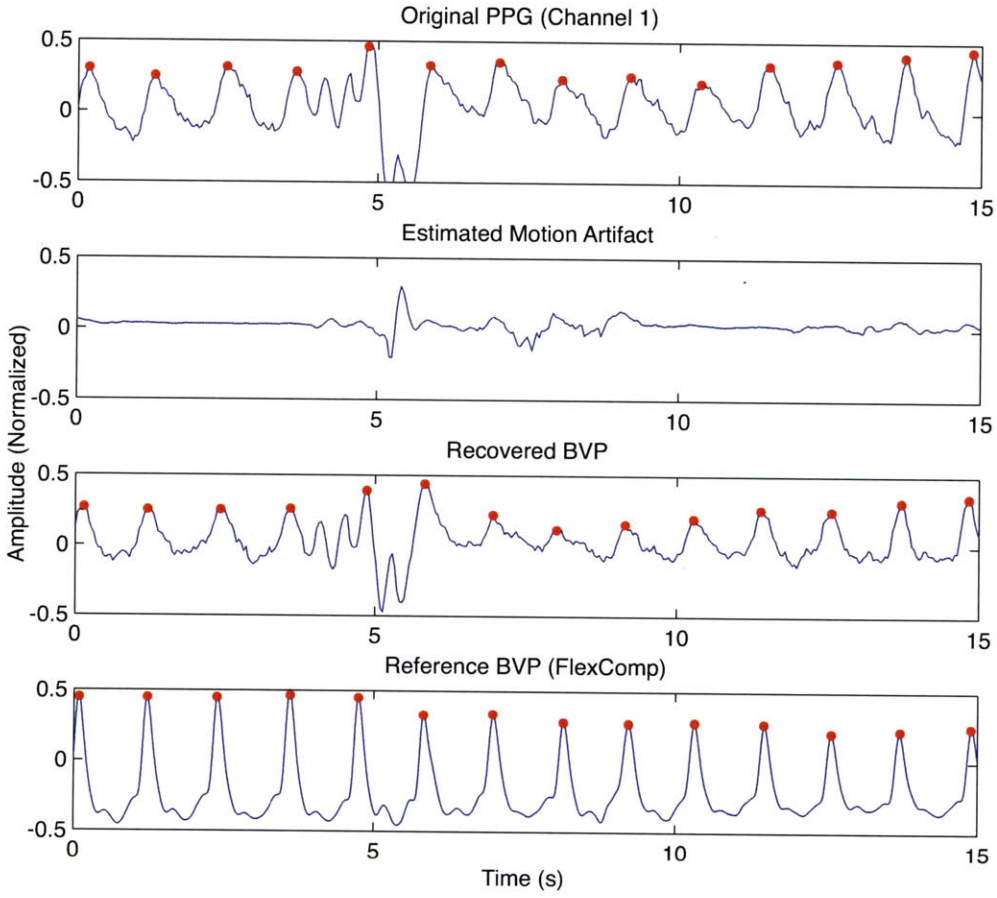

Figure 4-5: Motion artifact cancellation during a single grip motion.

Finally, the PPG sensor was worn for a few hours during normal activity, and the measured heart rate was compared to the Alive ECG sensor data. The figure shows the heart rate measurements of the two sensors, together with the accelerometer data from the wristband sensor. As shown on the plot, the PPG data deviates significantly from the ECG during walking. The motion artifacts introduced by the walking motion simply rails the signal to its dynamic range limits, and the heart rate cannot be recovered. However, while the user is working on a computer, the PPG heart rate tracks the ECG heart rate relatively well, except at times when there are significant movements due to typing or the use of the mouse. During work, there are many intervals when the person remains still while thinking

or reading, and this minimizes the motion artifacts and therefore the heart rate can be recorded fairly accurately. As the accelerometer reading shows, the amount of movement during sleep is almost negligible, and therefore the heart rate is measured very accurately.

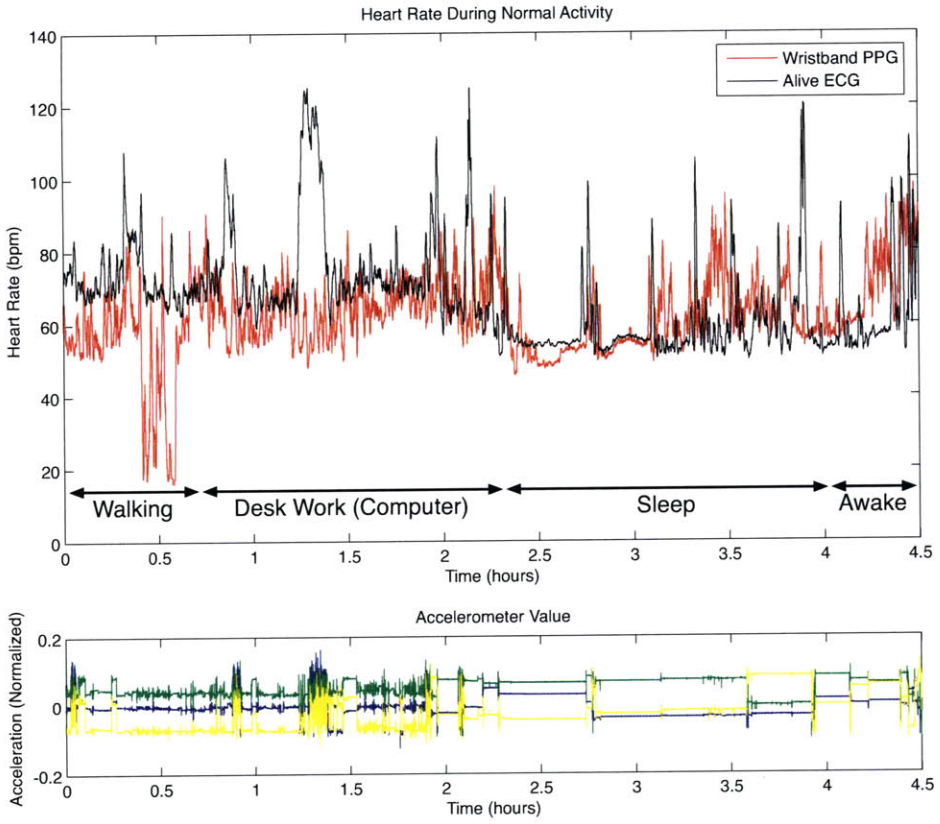

Figure 4-6: PPG and ECG heart rate measurement comparison during normal activity.

Also, an interesting observation was made during the evaluation, where the estimated motion artifact signal was occasionally inverted. When this occurs, instead of cancelling the motion artifacts from the original signal, the system unfortunately ends up boosting the motion artifacts and corrupting the signal even further. This occurs due to the inaccuracy in the assumption that the channel 1 SNR r_1 is always higher than the channel 2 SNR r_2. The reference cited in the theory chapter stated that the SNR is improved with brighter light sources[8]. However, it turns out that there is a difference between the noise N being background noise or motion artifact noise. In the case of background noise with no motion artifacts present, the brighter light source will simply boost the BVP signal (as background

noise remains constant) and the SNR improves. However, when the motion artifacts are present, the brighter light source may boost the motion artifacts together with the BVP signal, since they may both be volumetric changes under the skin.

In order to fix this, an alternative photodetector scheme must be developed, such that the relative SNR values of the two channels are well defined. One possible approach is to explore the use of different wavelengths to obtain a differential measurement[1]. If the SNR of the PPG signal using a certain wavelength is guaranteed to be higher (or lower) than that of another wavelength, the two wavelengths can be setup to provide a pair of signals with reliable SNR differences.

The complex modelling of the structure under the skin is not within the scope of this project. However, it is important to note that the motion cancellation system outlined in this thesis is valid regardless of the differential input signal source, and the system is designed in a modular manner that the current brightness based differential signal input may be replaced with any other pair of differential signals to function correctly. Therefore, the performance of this motion cancellation system may potentially be improved with further modelling of the reflection and absorption mechanism under the skin.

[1]See Appendix A "Alternative Differential Measurement Approaches" for details.

Chapter 5

Conclusions and Future Work

This thesis outlined the development of a novel motion artifact cancellation model for a wearable PPG sensor. Specifically, this work focused on improving the motion artifact cancellation performance by approaching the problem from the analog front-end sensor level, instead of the traditional DSP algorithms level. The motion artifact cancellation model is based on the idea of differential measurement and common-mode rejection, together with calibration and AGC stages to allow for any two PPG signals with different SNRs to perform the motion artifact cancellation.

The testing results indicate that the system performs very well when the motion artifacts are sustained for longer than 2 seconds, to allow for the AGC to catch up with the increased motion artifact signal level. The BVP peaks are clearly recovered and well-defined, even when the original PPG signal contains a significant amount of motion artifact ripple that the BVP peaks are ambiguous and difficult to determine. However, due to the delay caused by the AGC, the system does not perform as well for short motion artifacts that occur for less than 2 seconds, as the estimated motion artifact signal does not catch up to cancel out the motion artifacts in the original signal. Also, the estimated motion artifact signal occasionally inverts, due to the uncertainty in the relative SNR values of the two input signals, and this unfortunately results in boosting the motion artifacts.

Therefore, this system can potentially be improved in the future by incorporating a faster AGC system, and also by using an input PPG signal pair with well defined relative SNRs. Instead of using a closed loop feedback system, the AGC may be designed for faster performance in open loop, by accurately matching the average value reference to the

applied gain level using high precision components. Alternatively, if the AGC system can be implemented in digital, this may reduce the transient delay significantly, allowing the motion artifact cancellation to perform well even for short motion artifacts. The inversion of the estimated motion artifact can be prevented if the relative SNRs of the two input signals can be well defined, and this may be done by modelling and characterizing various types of input signal acquisition off the skin, such as using different wavelengths of light to obtain the two PPG signals.

5.1 Thoughts on Design Tradeoffs

The motion artifact cancellation system was designed in analog for the benefits of real-time processing, reduced complexity, and lower power consumption. However, as we saw in the discussion section, there are clear limitations with the analog implementation, mainly due to the limitations of the power supply rail. For improved AGC performance, it would make sense to implement the feedback loop in the digital domain, so that the control signals can be arbitrarily large.

However, the use of microprocessor consumes large amounts of power, and this added power consumption is usually orders of magnitude greater than the analog implementation. Also, the computational power required to implement the AGC or any other signal processing system may require more than one microprocessor, resulting in an even higher power consumption. Since low power consumption is an important factor to consider for a battery operated wearable sensor design, there is a major design tradeoff between performance and battery life.

Therefore, it may actually be the most optimal to use a hybrid design with both analog and digital components. Simple signal processing tasks such as applying gain or subtraction can easily be implemented with low power analog electronics. For complex signal processing tasks such as the AGC, microprocessors can be used for high performance implementation.

5.2 Generalization of Method

The motion artifact cancellation model was designed for PPG sensor signals. However, it is possible to extend the model further and generalize it as a signal isolation technique. For any given "black box" mixture of signals, a signal of interest (signal) can be isolated from

the rest (noise) if it satisfies the following conditions:

- The noise can be temporarily turned off for calibration
- The "black box" mixture can be separated into different channels with different SNRs
- The relative values of SNRs are well defined
- The input signal amplitude is within the dynamic range of the system rails
- The noise can be sustained for the duration of the transient settling time

5.3 Applications to Affective Computing

The generalized signal isolation technique may have potential applications in the field of affective computing, as a means to identify certain emotional states through physiological data. Previous research suggests that parameters such as heart rate, BVP amplitude, heart rate variability (HRV), and electrodermal activity (EDA) are influenced by the activation of autonomic nervous system (ANS) [1, 10, 11]. If patterns exist within the ANS activation for a given emotional state, and if there is a method to setup a physiological signal to calibrate for a particular emotional state, then it may be possible to extract the signal that identifies the emotional state of interest.

As mentioned in the introduction, the complete PPG signal model is given by [4]

$$S_{PPG} = S_{ambient} + S_{vascular} + S_{mechanical} + S_{electrical} \tag{5.1}$$

Since emotional states affect the behavior of many physiological parameters and symptoms appear in many parts of the body, we can assume that the $S_{vascular}$ term can be expanded into various emotion-dependent subcomponents.

For example, EDA is considered as a measure of arousal, which increases with the activation of the sympathetic nervous system [1, 10]. However, EDA does not give you the information on the parasympathetic nervous system, which is also a key parameter when analyzing ANS activity. With the use of the PPG sensor, the R-R intervals can be calculated to determine HRV, which contains both sympathetic and parasympathetic information.

Also, previous research suggests that the amplitude envelope of the PPG signal is influenced by stress and relaxation [11]. As a person relaxes, the amplitude envelope increases,

and vice versa. Since our sensor computes the average signal level for the AGC, we can potentially use this as a measure of changing amplitude envelope, and possibly infer the stress level of the user from this information.

Appendix A

Alternative Differential Measurement Approaches

Originally, the differential measurement model was inspired by the fact that using different wavelengths of light results in different SNR in the detected PPG signal [9]. For example, green light (λ = 570nm) has a much higher absorptivity for both oxyhemoglobin and de-oxyhemoglobin compared to infra-red light (λ = 700nm). This indicates that there is a greater change in reflected green light than in reflected infra-red light when blood pulses through underneath the skin, resulting in a better SNR for the green light source.

Using this approach, a differential measurement setup can be designed, where LED-photodetector pairs for green wavelength and infra-red wavelength are placed next to each other, such that the two photodetectors measure different BVP amplitudes, while they experience nearly identical motion artifacts. Using the mathmatical notation from chapter 2, the green channel will be $s_1 + n$, and the infra-red channel will be $s_2 + n$. If we can measure the difference between these two photodetector signals, the common-mode motion artifact can potentially be eliminated.

However, preliminary tests with this design demonstrated major issues with this model. The mismatch of the two channels were significant due to the fact that the two phototransistors were two different components (one at λ = 570nm and the other at λ = 700nm). To show this mathematically, the green channel v_1 and the infra-red channel v_2 can be represented as

$$v_1 = s_1 + n_1 \tag{A.1}$$

$$v_2 = s_2 + n_2 \tag{A.2}$$

The noise components are not identical, and the mismatch is significant enough that the two noise components are not scaled versions of each other

$$n_1 \neq k_n n_2 \tag{A.3}$$

This makes it impossible for the motion artifacts to cancel out. Therefore, a differential measurement approach using two identical phototransistors was used in the actual design.

Appendix B

Alternative Automatic Gain Control Approaches

There are many ways to design the blocks in the automatic gain control (AGC) system. The following are a few approaches that were considered, and the reasons why they could not be successfully incorporated in the AGC loop.

B.1 Emitter Coupled Pair

The first topology that was considered for a variable gain stage was an emitter coupled pair (an emitter follower stage followed by a common base stage). By applying the feedback voltage on the bottom end of the emitter resistor, the bias current of the emitter coupled pair can be changed to alter the g_m, which will proportionally alter the gain. However, the problem with this design is that as the bias current changes, the DC bias of the output voltage will change as well, and that transient of the moving DC bias couples through the output AC coupling stage to affect the average value of the output signal. This system will therefore never settle, and the loop is unstable.

B.2 Variable Gain Amplifier

Another way to implement the variable gain block is by using a variable gain amplifier (VGA). However, for a power rail of +3.3V, the only available VGAs were digitally controlled. It may be possible to add an ADC before the VGA to interface the analog control

voltage to the digital VGA, but this approach was much more complex compared to the OTA approach that was used in the final design.

B.3 Compandor

A compandor is a single IC that contains all of the blocks that are necessary for an AGC loop (variable gain, full-wave rectifier, and low pass filter). Such ICs may potentially be used to implement the whole AGC function. However, after extensive search for various compandor ICs, none were found that allowed access to the necessary pins to design a custom AGC loop. Most compandor ICs were designed using a fixed internal reference voltage to output a fixed amplitude signal, and they could not be modified to use an external reference.

B.4 Lag Compensator

Since our AGC application requires the steady-state error to be extremely low, a lag compensator with a pole at the origin can be used to eliminate the steady-state error completely. However, this approach has a major drawback in terms of the transient response, as lag networks typically have their characteristic slow rising transients, which can take a long time to reach the final value. The error caused by this slow transient will be similar to having a steady-state error, and therefore it is better to instead apply a large gain to reduce steady-state error and recover the stability using a lead network.

Bibliography

[1] R.R. Fletcher, K. Dobson, M.S. Goodwin, H. Eydgahi, O. Wilder-Smith, D. Fernholz, Y. Kuboyama, E.B. Hedman, Ming-Zher Poh, and R.W. Picard. icalm: Wearable sensor and network architecture for wirelessly communicating and logging autonomic activity. *Information Technology in Biomedicine, IEEE Transactions on*, 14(2):215 –223, march 2010.

[2] S.R. Quint, J.A. Messenheimer, M.B. Tennison, and H.T. Nagle. Assessing autonomic activity from the ekg related to seizure onset detection and localization. In *Computer-Based Medical Systems,1989. Proceedings., Second Annual IEEE Symposium on*, pages 2 –9, 26-27 1989.

[3] Ming-Zher Poh, Nicholas C. Swenson, and Rosalind W. Picard. Motion-tolerant magnetic earring sensor and wireless earpiece for wearable photoplethysmography. *Trans. Info. Tech. Biomed.*, 14(3):786–794, 2010.

[4] Phillip Andrew Shaltis. *A Wearable Blood Pressure Sensor Using Oscillometric Photoplethysmography and Micro Accelerometers.* PhD thesis, Massachusetts Institute of Technology, 2007.

[5] L.B. Wood and H.H. Asada. Low variance adaptive filter for cancelling motion artifact in wearable photoplethysmogram sensor signals. In *Engineering in Medicine and Biology Society, 2007. EMBS 2007. 29th Annual International Conference of the IEEE*, pages 652 –655, 22-26 2007.

[6] P. Renevey, R. Vetter, J. Krauss, P. Celka, and Y. Depeursinge. Wrist-located pulse detection using ir signals, activity and nonlinear artifact cancellation. In *Engineering in Medicine and Biology Society, 2001. Proceedings of the 23rd Annual International Conference of the IEEE*, volume 3, pages 3030 – 3033 vol.3, 2001.

[7] Jianchu Yao and S. Warren. A short study to assess the potential of independent component analysis for motion artifact separation in wearable pulse oximeter signals. In *Engineering in Medicine and Biology Society, 2005. IEEE-EMBS 2005. 27th Annual International Conference of the*, pages 3585 –3588, 2005.

[8] P. Branche and Y. Mendelson. Signal quality and power consumption of a new prototype reflectance pulse oximeter sensor. In *Bioengineering Conference, 2005. Proceedings of the IEEE 31st Annual Northeast*, pages 42 – 43, 2-3 2005.

[9] WG Zijlstra, A Buursma, and WP Meeuwsen van der Roest. Absorption spectra of human fetal and adult oxyhemoglobin, de-oxyhemoglobin, carboxyhemoglobin, and methemoglobin. *Clinical Chemistry*, 37(9):1633–1638, 1991.

[10] Hoda Eydgahi. Design and evaluation of icalm: A novel, wrist-worn, low-power, low-cost, wireless physiological sensor module. Master's thesis, Massachusetts Institute of Technology, 2008.

[11] R. Fernandez and R.W. Picard. Signal processing for recognition of human frustration. In *Acoustics, Speech and Signal Processing, 1998. Proceedings of the 1998 IEEE International Conference on*, volume 6, pages 3773 –3776 vol.6, 12-15 1998.